



Classifying benthic habitats in the shallow water around St. Eustatius using remote sensing

MSc. Thesis

Student: Iris van Rijn

Email: i.vanrijn1@students.uu.nl

Supervisors:
dr.ir. Jan Clevers
dr.ir. Sander Mûcher
dr. Erik Meesters

23-02-2024



Acknowledgements

For my thesis I wanted to choose a project that covered my interest in both GIS and biology. After stumbling upon this subject I was immediately enthusiastic, although I had little experience with remote sensing. This thesis was not possible without the trust and enthusiasm of my supervisors Jan Clevers, Sander Mucher and Erik Meesters.

I would like to thank Sander Mucher and Erik Meesters for their input during meetings and knowledge on St. Eustatius. I have learned a lot from your ideas and got excited on the subject. Finally, I would like to thank Jan Clevers for his supervision during this thesis. Thank you for the guidance and feedback and for the quick response when I got stuck on technical issues. I am glad to have been your final thesis student and I want to wish you a happy retirement.

Abstract

This research aims to create a benthic habitat map of the shallow water (<30m) around St. Eustatius using high-resolution multispectral WorldView-3 imagery and in situ observations. Various classification algorithms are explored and the effect of sunglint correction and water column correction on classification were examined. Additionally, the research investigates the detectability of changes in benthic habitat composition between 2009 and 2018.

To improve the original imagery, preprocessing steps are performed including sunglint removal and water column correction. Due to limited amount of sunglint, sunglint removal performed poorly, resulting in reduced variation in the deeper part of the imagery. Water column correction however, showed more promising results. When creating a Depth-Invariant Index of the blue (450-510 nm) and green (510-580 nm) spectral band, structures in deeper water showed more clearly than in the original multispectral image. However, despite visible improvements, overall classification accuracy remains lower compared to classification of the original imagery.

After preprocessing one unsupervised and four supervised classification algorithms are compared. Unsupervised classification algorithms can be used to segment the imagery without prior training data. The results of the ISODATA (Iterative Self-Organizing Data Analysis Technique) classification show that its accuracy is comparatively lower than supervised algorithms. However, it could be a valuable tool for initial exploration and identification of habitat patterns. Supervised classification algorithms, such as Maximum Likelihood Classifier (MLC), Random Tree (RT), K-Nearest Neighbor (K-NN), and Support Vector Machine (SVM), were better able to classify benthic habitats with accuracies ranging from 56.9% - 67.3%. SVM performed best visually in classification of the water column corrected image and represents each of the habitat classes more evenly compared to the other classifiers.

Lastly, an attempt at change detection is done by visually comparing imagery of 2009 and 2018. The results show potential shifts in benthic composition, which highlights the importance of regular monitoring. This research indicates that integration of up-to-date in situ data with high-resolution satellite imagery has high potential for identifying and classifying benthic habitats around St. Eustatius.

Keywords: St. Eustatius, Benthic habitats, Remote sensing, WorldView-3

Table of contents

1. Introduction	7
1.1 Research objectives	8
2. Literature review.....	9
2.1 Spectral characteristics of benthic objects	9
2.2 Satellite characteristics	9
2.3 Benthic habitat mapping	10
2.3.1 Preprocessing techniques	10
2.3.2 Classification techniques	11
3. Methodology.....	12
3.1 Study area	12
3.2 Data.....	13
3.2.1 Satellite imagery	13
3.2.2 Ground truth data.....	13
3.3 Conceptual model	16
3.4 Preprocessing steps	17
3.4.1 Masking of image	17
3.4.2 Radiometric correction and atmospheric correction	17
3.4.3 Sun glint correction.....	17
3.4.4 Water column correction	18
3.5 Preparation in-situ data	19
3.6 Image classification	20
3.6.1 Iterative Self-Organizing Data Analysis Technique (ISODATA)	20
3.6.2 Maximum Likelihood Classifier (MLC).....	20
3.6.3 Support Vector Machine (SVM).....	20
3.6.4 K-Nearest Neighbor (K-NN)	20
3.6.5 Random Trees (RT)	21
3.7 Accuracy assessment	21
3.8 Additional analysis	22
3.8.1 Depth-Invariant Index bands coastal blue & green.....	22
3.8.2 Training data.....	22
3.8.3 Object-based classification	22
3.9 Comparison between 2009 and 2018.....	22
4. Results	23
4.1 Preprocessing steps	23
4.2 Image classification.....	26
4.2.1 Iterative self-organizing data analysis technique (ISODATA)	26

4.2.2 Maximum Likelihood Classifier (MLC)	27
4.2.3 K-Nearest Neighbor (K-NN)	28
4.2.4 Support Vector Machine (SVM)	28
4.2.5 Random Tree (RT)	29
4.3 Accuracy assessment	29
4.4 Additional analysis	31
4.4.1 Depth-Invariant Index bands coastal blue and green	31
4.4.2 Training data	31
4.4.3 Object-based classification	32
4.5 Comparison between 2009 and 2018	33
5. Discussion	35
5.1 Characteristics of the data	35
5.2 Preprocessing steps	35
5.2.1 Sunlint removal	35
5.2.2 Water column correction	36
5.3 Classification algorithms	37
5.4 Comparison between 2009 and 2018	38
6. Conclusions and recommendations	39
6.1 Sub questions	39
6.2 Recommendations	41
7. References	42
8. Appendices	47
Appendix A - Results of the ISODATA classification	47
Appendix B – RGB image and ISODATA classification after water column correction	48
Appendix C – ISODATA classification of 2009 imagery after sunlint removal	48
Appendix D - Confusion matrices for five classifiers	49
ISODATA	49
MLC	49
K-NN	49
SVM	50
RT	50

List of Figures

Figure 1 - In situ optical reflectance spectra R of coral reef benthic communities. The white line in each shows mean spectra for the bottom-type (Hochberg et al., 2003a).....	9
Figure 2 - Location of St. Eustatius in the Caribbean sea.....	12
Figure 3 - Map of the protected areas of St. Eustatius (Smith, 2008).....	12
Figure 4 - Ground truth data points containing observed benthic habitat located on the map.....	13
Figure 5 - Benthic seascape map of St. Eustatius, created from ground truth data (Debrot et al., 2014)	13
Figure 6 - Benthic habitat types in St. Eustatius. Images and descriptions are from Debrot et al. (2014).....	15
Figure 7 - Conceptual model for this research Green boxes are data sources, blue boxes are data outputs and white boxes are steps to be take. The classification algorithms used in this research are ISODATA (Iterative Self-Organizing Data Analysis Technique), MLC (Maximum Likelihood Classifier), K-NN (K-Nearest Neighbour), SVM (Support Vector Machine) & RT (Random Trees)	16
Figure 8 - Processes of water column correction (Green et al., 2000).....	18
Figure 9 - General workflow supervised and unsupervised classification.....	20
Figure 10 - Areas selected for deglinting of the image. Source: DigitalGlobe. WorldView-3, ORTStandard2A level, 19 Nov, 2018.....	23
Figure 11 - Bi-plots of areas selected for deglinting of pixel values of water penetrating bands against the NIR band and their slopes, reflectance is given in 11-bit pixel value	24
Figure 12 - Coastal band after sunglint removal using NIR-1 (left) and NIR-2 (right). Source: DigitalGlobe. WorldView-3, ORTStandard2A level, 19 Nov, 2018.....	24
Figure 13 - Results before (left) and after (right) sunglint removal. Source: DigitalGlobe. WorldView-3, ORTStandard2A level, 19 Nov, 2018.....	24
Figure 14 – Depth-Invariant Index of bands 2 and 3 compared to Depth-Invariant Index of bands 1 and 3. Source: DigitalGlobe. WorldView-3, ORTStandard2A level, 19 Nov, 2018.....	25
Figure 15 - Results of unsupervised classification ISODATA on MS (top) and DII_23 (bottom).....	26
Figure 16 - Results ISODATA on blue band (left) compared to DII_23 (right) (see Fig 15 for legend)	27
Figure 17 - Results MLC on MS (left) and DII_23 (right) (see Fig 15 for legend)	27
Figure 18 - Results K-NN on MS (left) and DII_23 (right) (see Fig 15 for legend).....	28
Figure 19 - Results SVM on MS (left) and DII_23 (right) (see Fig 15 for legend)	28
Figure 20 - Results RT on MS (left) and DII_23 (right) (see Fig 15 for legend).....	29
Figure 21 - SVM classification for DII 13 and DII 23 (see Fig 15 for legend)	31
Figure 22 - SVM classification with 'original' training data (left) and with 'enhanced' training data (right) (see Fig 15 for legend)	32
Figure 23 - Segmented raster (left) and SVM object-based classification (right) on DII_13 (see Fig 15 for legend).....	32
Figure 24 - Original satellite imagery (left) and after clipping (right). Source: DigitalGlobe. WorldView-2, ORTStandard2A level, 6 Dec, 2009.	33
Figure 25 – Structure in the water shown in the blue band of 2009 imagery before (left) and after (right) sunglint removal. Source: DigitalGlobe. WorldView-2, ORTStandard2A level, 6 Dec, 2009.	33
Figure 26 – Comparison of four apparent structures (A,B,C,D) found in the same locations in 2009 and 2018.	34
Figure 27 - Mean spectral profile before and after sunglint removal	35
Figure 28 - Comparison of underwater reflectance values of different benthic covers with the corresponding band (Tamondong & Blanco, 2017)	36
Figure 29 - Comparison of SVM classification of the apparent structures on MS (top), DII_13 (middle), DII_23 (bottom).....	37

List of Tables

Table 1 - WorldView band parameters	13
Table 2 - Parameters used for performing water column correction	25
Table 3 - Overall accuracies and accuracy per class for five classification methods	29
Table 4 - Calculated metrics for five classifiers.....	29
Table 5 - Overall accuracies and accuracy per class for DII_13 and DII_23	31
Table 6 - Number of samples and percentage of pixels before (left) and after (right) training data removal.....	31
Table 7 - Accuracy assessment SVM before and after altering training data.....	32
Table 8 - Accuracy assessment SVM object-based classification.....	32

1. Introduction

Shallow coastal waters represent some of the most important environments of the ocean (Micallef et al., 2012). They are often complex structures that consist of a number of different benthic habitats. As part of these habitats, coral reefs are biologically diverse ecosystems that provide many services including food, jobs and income for coastal communities and coastal protection (Moberg & Folke, 1999; Lam et al., 2019). However, due to climate change and human activities such as pollution and overfishing, the resilience of benthic life is pushed towards their limit (Glasl, Webster & Bourne, 2017). This can cause alterations in benthic cover and structural complexity, which is strongly linked to the diversity, abundance and biomass of reef fishes (Graham & Nash, 2013).

The condition of coral reef ecosystems in the Caribbean is rapidly declining. Already two-third of the reefs was threatened by 2003 (Mishra et al., 2006). The resulting damage from these declines are a low fish population together with outbreaks of coral diseases, making it difficult for coral to recover (Wilkinson & Souter, 2008). St. Eustatius is part the northern Leeward Islands in the Caribbean sea, next to Saint Kitts and Saba. The island still has exceptionally healthy marine ecosystems and coral cover and is important for biodiversity, conservation and tourism (Bervoets, 2010). According to Debrot et al. (2014), 41% of the benthic habitat surrounding St. Eustatius is estimated to be reef. Since the islands of the Caribbean are very dependent on their reefs resources, it is important to put effort towards conservation and better management.

A tool that is used more often to assess and monitor coastal marine systems are benthic habitat maps. These maps provide knowledge on the spatial distribution and on the quality of the habitats (Micallef et al., 2012). This knowledge gives us the ability to protect the reef from anthropogenic impacts. Optical remote sensing is a method that can be used to create habitat maps by measuring the solar reflectance of those habitats at a distance. Synoptic information sources such as satellite imagery can be obtained in a high temporal frequency, which improves the accuracy of determining the effects of anthropogenic impacts on coral reef (Foo & Asner, 2019). It is however limited to the shallow water because of attenuation of the light in the water column. Nevertheless, the upper layer of the ocean is the most productive layer of the ocean. This means that having knowledge of the upper layer, could provide information on the deeper ocean as well (Kachelriess et al., 2014).

Historically, field-based monitoring from divers' observation and the gathering of samples has been a broadly applied method to create habitat maps. These surveys are costly, time consuming and limited to the accessible parts of the water (Micallef et al., 2012). Geographically limited areas could be shallow water, dangerous areas with reefs or rocks or dynamic zones where a high frequency of surveys is necessary to have up-to-date data, which could be very expensive (Kutser et al., 2020). Remote sensing can scale-up the amount of in-situ observations in an area since it is less time consuming and expensive (Mumby et al., 2004). According to Foo & Asner (2019), remote sensing is a good technology for recognizing widespread subtle changes in coral cover over time.

The potential for habitat mapping from multispectral satellite data with high spatial resolution comes from the ability to identify individual components based on their spectral response (Mishra et al., 2006). However, benthic habitat mapping with remote sensing techniques also imposes challenges. The spectral signal for a habitat type is subjected to other variations in an image such as for example suspension of sediments (Hedley et al., 2012). Therefore, it could be a challenge to distinguish between spectral response in a remotely sensed image, limiting the quantification of benthic cover (Foo & Asner, 2019). In addition to this, depth plays a significant role in the ability to identify different benthic types. Absorption and backscattering effects in the water column complicate analysis. When depth increases, so does scattering and absorption, reducing the signal strength across all wavelengths (Rowan & Kalacska, 2021). Obtaining accurate bathymetric data is therefore a challenge especially for shallow coastal waters where multibeam hydrographic surveys are often complicated.

When satellite imagery is acquired, it can not directly be used for analysis because of influences from for example the sensor and atmosphere (Xu et al., 2019). Several preprocessing steps are required to correct the images before use. Since the specifications of each satellite differ, so does the processing and classification of the images. In this research, WorldView-3 imagery is corrected and classified with the use of in situ data to create a benthic habitat map of the water around St. Eustatius, also known as Statia.

1.1 Research objectives

The objective of this research is to use high-resolution multispectral WorldView-3 (WV-3) imagery to create a benthic habitat map of St. Eustatius. Based on this objective, the following research question and sub questions are formulated:

To what extent can benthic habitats of St. Eustatius be accurately mapped using in situ data and WorldView-3 imagery?

Sub questions:

- Which classification algorithms are most suitable for benthic habitat mapping of shallow waters (<30m)?
- What is the effect of correcting for water depth to benthic habitat classification of WV-3 imagery?
- Can change in the composition of benthic habitats be detected from WV imagery between 2009 and 2018?

There are many algorithms available for the classification of high resolution optical satellite data. In this research both supervised- and unsupervised classification algorithms will be compared to select the most suitable classification algorithm. For the definition of shallow water, 30m has been selected as the maximum depth. Hyperspectral imaging is in general best applicable to the identification of habitat characteristics at less than 20m depth (Foo & Asner, 2019). Light scattering in the water column decreases with increasing wavelength due to increased absorption, with scattering of wavelengths longer than blue already being negligible (Rowan & Kalacska, 2021). WorldView-3 has an additional band called “Coastal blue” (400-450 nm) with smaller wavelengths than blue (450-510 nm). In addition to this, the densest coral around Statia is concentrated around 24m depths (Debrot et al., 2014). Therefore, it is decided to define water up to 30 meters as shallow.

The influence of water depth on absorption and scattering of light has already been discussed. Water column correction is a widely used method to reduce this impact on classification results. However, the real values of water column parameters at the moment the image was taken are often unknown. According to a comparison of classification algorithms on WorldView-3 imagery with and without water column correction by Mederos-Barrera et al. (2022), only minor improvements are made in calm, clear and shallow waters. Therefore, it is interesting to see how it affects classification in the water around Statia.

The last sub question is formulated because WorldView-2 imagery of the water surrounding Statia is available, acquired in 2009. This data is used to make a comparison with the more recent WorldView-3 imagery.

2. Literature review

2.1 Spectral characteristics of benthic objects

The radiance that is measured from optical remote sensing over water bodies originates from sunlight and is scattered, absorbed and reflected by particles in the water, before passing through the atmosphere and returning to the sensor (Arora et al., 2018). The scattering, absorbing and reflecting of particles in the water has a large effect on the spectral signature of objects in water. In coastal waters, there are three elements that influence this effect, chromophoric dissolved organic material (CDOM), phytoplankton photosynthetic pigment chlorophyll-a (Chl-a), and total suspended matter (TSM) (O'Neill et al., 2011). The effect of each of these three elements is wavelength dependent and increases with depth. CDOM absorbs light in the blue spectral range, Chl-a absorbs light in the blue and red spectral range and TSM increases reflectance in the red spectral range and shifts the peak in the green spectrum. These attenuations of light in the water column affect the reflectance patterns in various ways (Hochberg et al., 2003a).

A coral reef community consists of several elements including corals, seagrass, various algae and sand. Each substrate type has a distinguished functional role in an ecosystem and distinguished spectral characteristics that can be used to separate it from other objects (Figure 1). For example, in situ measurements of sand show high reflectance in comparison to other substrates reaching from 20% at 400 nm to 80% at 700 nm (Hochberg et al., 2003a) and seagrasses have a broad reflectance peak between 550-560 nm because of their green colour, corresponding to the green spectral band that ranges from 510 to 580 nm. Because of objects having different characteristics, there is the ability to differentiate between classes with remote sensing. However, classification errors do occur. Reflectance of coral for example, is dependent on pigments that are found in a coral colony (Hochberg et al., 2003b). These structures are complex and result in some variability between corals. Therefore, classification errors can occur but are often within a certain bottom-type and not between bottom-types. With as few as four narrow wavebands, separation of basic bottom types such as coral, algae and sand can be realised (Hochberg et al., 2003b).

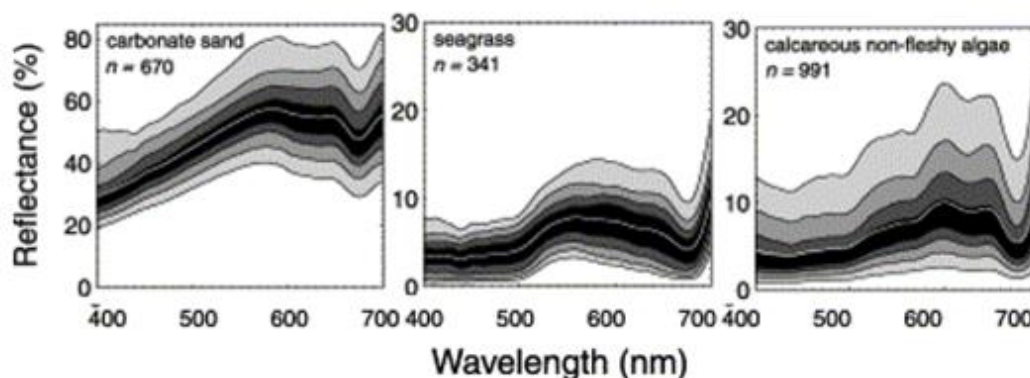


Figure 1 - In situ optical reflectance spectra R of coral reef benthic communities. The white line in each shows mean spectra for the bottom-type (Hochberg et al., 2003a)

2.2 Satellite characteristics

The ability to separate bottom types is also dependent on satellite characteristics. First of all, the acquisition rate of a satellite is an important factor. A useable amount of images for the monitoring of disturbances is estimated to be around 20 images per year (Hedley et al., 2018). However, useable images mean that the impact of cloud and sunglint is negligible. Weather conditions can also limit the applicability of optical remote sensing, since waves causes turbidity of water, which makes it more difficult to see through the water. Therefore, a satellite with a high revisit time is more likely to return sufficient useable images for comparison. Furthermore, the spatial resolution is another characteristic that influences the ability to separate habitat classes. Although the use of images from several spatial resolutions, ranging from <10 meters from Quickbird imagery to 10-100 meters from Landsat imagery, has all resulted in successful mapping, it is still an important consideration for benthic mapping (McIntyre et al., 2017). Spectral mixing of image pixels can occur with a lower spatial resolution and can result in inaccurate classification. On the other hand, a high spatial resolution means more storage and

processing power and is therefore more costly. Lastly, the spectral resolution is of importance for benthic mapping. Wavelengths larger than 600 nm are no longer visible at a depth of 3.7 meter (McIntyre et al., 2017). Therefore, the spectral resolution is dependent on the amount of bands containing wavelengths of less than 600 nm. The WorldView-3 satellite is an example of a satellite that provides two extra bands to the traditional blue, green and red, which are coastal blue (400-450 nm) and yellow (585-625 nm). The addition of these extra bands increases the spectral resolution and is therefore able to improve classification accuracies (McIntyre et al., 2017).

2.3 Benthic habitat mapping

2.3.1 Preprocessing techniques

2.3.1.1 Atmospheric correction

Atmospheric correction has proven to be a crucial point in the pre-processing of images in remote sensing applications. Radiation undergoes absorption and scattering by particles in the atmosphere, resulting in a different measurement of reflectance compared to the true reflectance of the surface (Green et al., 2000). The effect of scattering by particles in the atmosphere is most noticeable in the blue end of the visible spectrum due to Rayleigh scattering (Tyagi & Bhosle, 2011). To account for this effect, there are several atmospheric correction techniques, different in complexity and their assumptions. Common ones include 6S (Second Simulation of the Satellite Signal in the Solar Spectrum), MODTRAN (Moderate Resolution Atmospheric Radiance and Transmittance Model), LOWTRAN and de The dark object subtraction (DOS) (Ding et al., 2015). The first three models are complex, since they require atmospheric data from the moment the imagery is acquired. The DOS only requires information contained in the digital image and is therefore more simple and is also proven to perform successfully (Abasolo et al., 2012). By applying atmospheric correction on imagery, the effect of the atmosphere that contributes to the signal that is measured by a satellite sensor is minimized.

2.3.1.2 Sunglint correction

Sunglint forms white bands in images on wave edges due to specular reflection of light from the water surface, when the water orientation at the surface directly reflects the sun towards the sensor (Hedley et al., 2005; Kay et al., 2009). These bands result in unusually bright pixel values, leading to incorrect image classification. The amount of sunglint in an image is dependent on factors such as surface roughness, the angle of the observation and the transparency of the atmosphere at the time the image is acquired (Lebedev & Zapralov, 2019).

To minimize the effect of sunglint, several methods are developed. For pixel sizes of less than 10m, information from the NIR band is usually used to indicate the amount of sunglint. It is assumed that the radiance in the NIR part of the spectrum that leaves the water is negligible and therefore any NIR that is recorded after atmospheric correction is due to sunglint (Kay et al., 2009). To establish this relationship between the NIR band and another band, a region in the deep water of the imagery is used, where the influence of NIR is expected to be zero.

2.3.1.3 Water column correction

In addition to radiometric, atmospheric and sunglint correction, benthic habitats might benefit from an additional pre-processing step since the depth of water significantly affects remotely sensed measurements. As depth increases, it becomes harder to separate habitat spectra (Green et al., 2000). Water is assumed to be homogenous, meaning that all bottom reflectance's are attenuated in the same way by the water column (Minghelli-Roman & Dupouy, 2014). Therefore, variation in the reflection of the seabed is only due to depth. To account for the effect of depth on bottom reflectance, knowledge of the attenuation characteristics of the water column and a depth measurement of every pixel are necessary (Mumby et al., 1997). Since accurate elevation models are often not available, the effect has to be compensated for in another way.

There are various techniques to correct for depth, ranging from simple to more complex algebraic algorithms. Lyzenga's algorithm (Lyzenga, 1981) is one of the most used algorithms and is relatively simple since it doesn't require knowledge of different water quality parameters (Mederos-Barrera et al., 2022). Lyzenga's model assumes that radiation exponentially decays with increasing depth due to light attenuation and that there are no substantial changes in water quality (Mumby et al., 1997). There are more accurate correction methods, but due to a lack of availability of optical water parameters especially in developing countries, Lyzenga's algorithm is widely applied.

2.3.2 Classification techniques

Classification algorithms can be divided in pixel-based classification and object-based classification. With pixel-based classification, individual pixels are directly classified while with object-based classification, pixels are first grouped into image objects with the use of segmentation algorithms before the objects are classified. Most previous research on benthic habitat mapping was conducted using pixel-based classification techniques. Pixel-based classification could potentially benefit from smoothing of the raster, to eliminate small and isolated areas (Micallef et al., 2012). These isolated pixels might not represent a different habitat structure and could therefore lead to misclassification. Object-based classification is assumed to be able to increase the accuracy (Wahidin et al., 2015). On the other hand, object-based classification also has its limitations. In benthic mapping, defining objects could be difficult. Therefore, it is possible to either under-segment or over-segment an image, leading to image objects that cover more than one class or classification errors such as a wrong area or shape (Liu & Xia, 2010).

Image classification can also be divided in supervised and unsupervised classification. Supervised classification involves the use of training data to assign a class value to a set of pixels. Both supervised- and unsupervised classification algorithms have been used for benthic habitat mapping. In previous research on mapping bottom-types in shallow water, supervised classification has shown to have a higher accuracy in comparison to unsupervised classification (Manessa et al., 2014). When using supervised classification, training sites need to be selected. These are areas in the image of known identity for each of the categories. The more training sites that are selected, the better the results will be (Perumal & Bhaskaran, 2010). Then signatures are extracted from these training sites and other pixels are assigned to the closest class from the training data.

3. Methodology

In this section the method used to carry out this research is explained. First, the study area and its marine parks are described. Then follows a description of the satellite data and the ground truth data that are used for this research. Lastly, the conceptual model of the research (Fig 7) is provided with an elaboration on all of the steps.

3.1 Study area

St. Eustatius is part of the Windward Islands of the Netherlands Antilles and is located in the Caribbean Sea (Fig 2). It is a volcanic island with an area of 21 km² and has a population of approximately 3,500 (Davies & Piontek, 2017). The northern part are steep rocky hills and the southern part is dominated by a volcano that rises 600 meters above sea level. On the ancient remains of these lava flows, coral reefs are formed surrounding the island (Smith, 2008). Furthermore, the marine environment consists of sea grass beds, rocky shores, sand and wrecks. The seafloor is shallow along the coast and slopes gradually till 50m. From here it quickly drops till depths of 200-300m (Davies & Piontek, 2017). There is also a difference between the conditions on the eastern and western side of the island. On the east there are strong winds and waves while the western coast has a lot calmer seas.

In order to manage the marine environment and other protected areas on Statia, the St. Eustatius National Parks Foundation (STENEPA) was established in 1988 (Smith, 2008). The protected marine park surrounds the whole island (Figure 3) but has two reserves that are actively being managed, the Northern and the Southern reserve. In these reserves, most of the coral reef is located and therefore anchoring and fishing is not allowed (Davies & Piontek, 2017). In the area between the two reserves, anchoring is allowed, resulting in a substrate of mainly rubble and algae.



Figure 2 - Location of St. Eustatius in the Caribbean sea

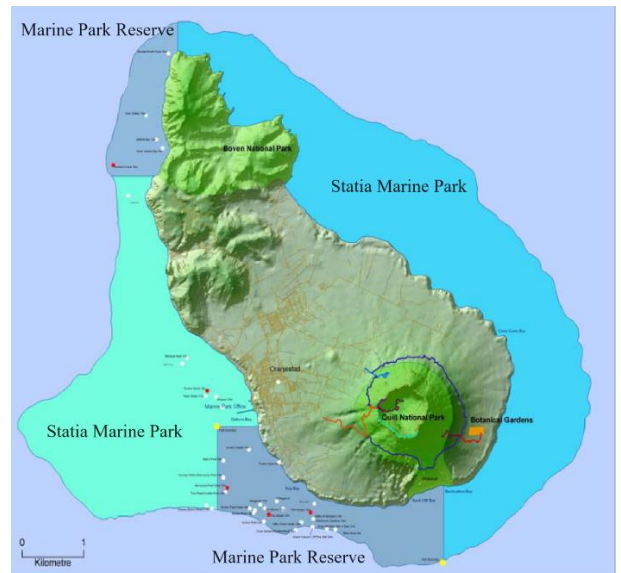


Figure 3 - Map of the protected areas of St. Eustatius (Smith, 2008)

3.2 Data

3.2.1 Satellite imagery

The main imagery available for this research is acquired in 2018 from the WorldView-3 satellite. This satellite has an altitude of approximately 617 km and a revisit time of 4.5 days at 20 degrees off-nadir angle. The spatial resolution for commercially available products are resampled to 0.31m for the panchromatic band and 1.24m for multispectral bands (Kuester, 2016) The wavelength range for each band is provided in Table 1. The WorldView-2 satellite that is used for comparison has an altitude of of 770 km and a revisit time of 3.7 days at 20 degrees off-nadir angle. The imagery available from 2009 has a spatial resolution of 0.46m for the panchromatic band and 1.85m for multispectral bands. Both satellties acquire data in 11-bit/pixel for panchromatic and multispectral bands, but store it as 16-bit integers to reduce file size

Both satellite images are delivered in ORTStandard2A level, meaning that atmospheric correction and orthorectification of the image is already applied. Maxar (the operator of WorldView) uses ACOMP for atmospheric correction, minimizing the effect of haze and vapor particles while providing normalized surface reflection values across every pixel, ranging from 0 to 2047.

Table 1 - WorldView band parameters

Band number	Waveband name	Wavelength range (nm)
1	Coastal Blue	400-450 nm
2	Blue	450-510 nm
3	Green	510-580 nm
4	Yellow	585-625 nm
5	Red	630-690 nm
6	Red Edge	705-745 nm
7	Near-IR1	770-895 nm
8	Near-IR2	860-1040 nm

3.2.2 Ground truth data

The ground truth data available for this research, is from a field campaign from Debrot et al. (2014). By following a transect line and recording video shots and a GPS-waypoint at every 150 meters, 524 location points are obtained with information on location, depth, and habitat. The depth of the video shots ranges from approximately 5 to 30 meters. Figure 4 shows the location of the ground truth data on the map. The majority of the field data is located on the south-western part of the shallow water around Statia.



Figure 4 - Ground truth data points containing observed benthic habitat located on the map

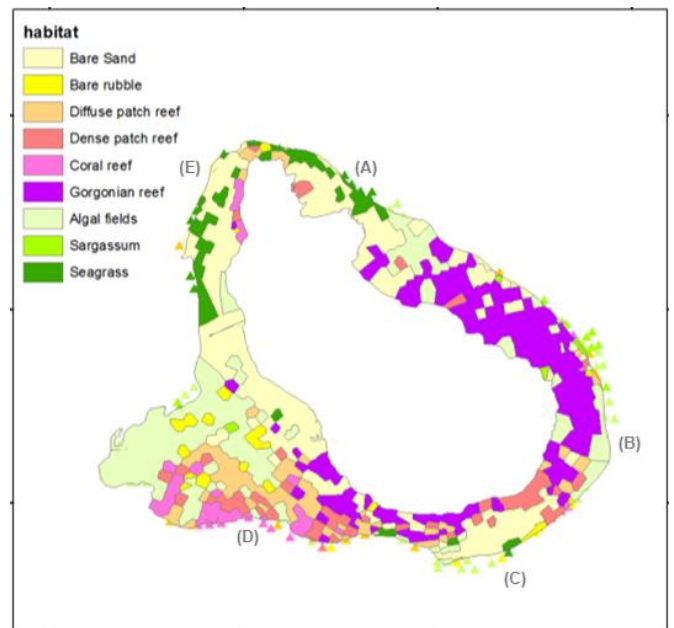


Figure 5 - Benthic seascape map of St. Eustatius, created from ground truth data (Debrot et al., 2014)

The substrate types that were determined on this field campaign were either sand, rock or rubble. These substrate-types were further specified to coral, gorgonian, sargassum, seagrass and algae depending on the benthic coverage of a 3 meter radius around the drop point. A benthic seascape map is created from the field campaign showing the different patterns in habitat around Statia (Figure 5).

The eastern side of the island (Fig 5A,B) is exposed to a lot of waves and wind, therefore having limited growth of benthic species. It does however contain Gorgonian coral species, since these are flexible and therefore able to withstand this movement. The western side of the island (Fig 5D,E) is more sheltered from the winds. It has a combination of rubble fields, with algae growing on it as well as corals and seagrass patches. Figure 6 contains a photographic sample of each seascape habitat containing a brief description from the report of Debrot et al. (2014).

- 1 - Unconsolidated Sediment
 - 1.1 Sand
- 2 - Coral Reef & Hard bottom
 - 2.1 Rubble
 - 2.2 Coral reef and gorgonian
- 3 - Seagrass and algae
 - 3.1 Seagrass and algae
 - 3.2 Sargassum sp.



Bare sand - No coverage of benthic species. Mostly found close to shore or between coral and gorgonian patches



Bare rubble - Almost no living coverage



Coral reef - A combination of different sponges, corals and algae



Gorgonian reef - Reef dominated by gorgonian species such as sea fans, wire coral sea plumes and sea fingers



Algal fields - Habitats overgrown by different algae species, often found between sand and reef



Seagrass fields - Sand patches covered by different seagrasses



Sargassum- A species of algae containing flotation organs, found on rubble.

Figure 6 - Benthic habitat types in St. Eustatius. Images and descriptions are from Debrot et al. (2014).

3.3 Conceptual model

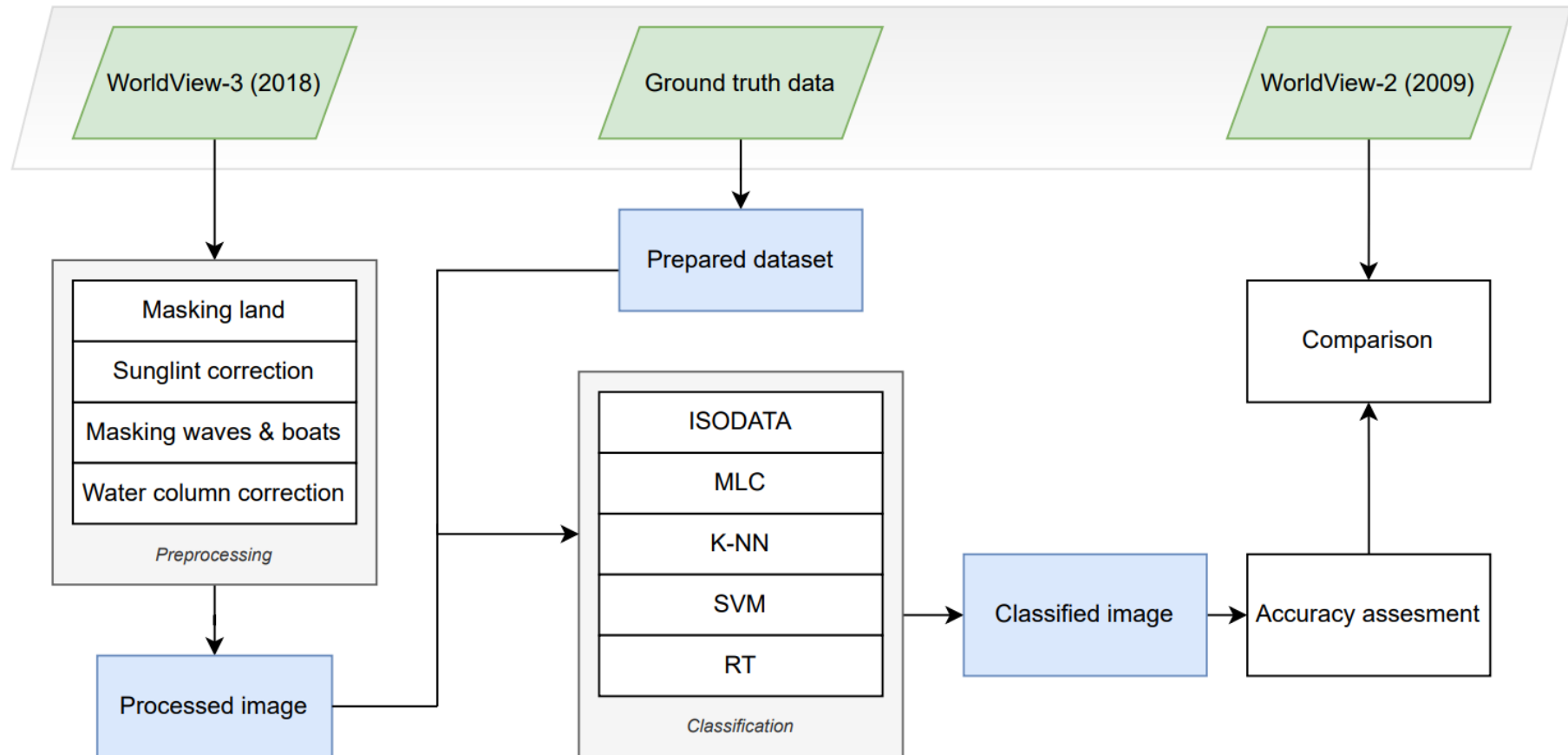


Figure 7 - Conceptual model for this research Green boxes are data sources, blue boxes are data outputs and white boxes are steps to be take. The classification algorithms used in this research are ISODATA (Iterative Self-Organizing Data Analysis Technique), MLC (Maximum Likelihood Classifier), K-NN (K-Nearest Neighbour), SVM (Support Vector Machine) & RT (Random Trees)

3.4 Preprocessing steps

Firstly, preprocessing is performed on the WV-3 imagery. Preprocessing steps consists of masking of the image, radiometric correction, atmospheric correction, sunglint correction and water column correction. After these steps are completed, classification can be done.

3.4.1 Masking of image

Image masking is done to remove irrelevant components for this research, such as land and deep water. The land pixels are masked by clipping the raster using a polygon created for previous research on St. Eustatius. To remove the deep water, a mask is created from a bathymetry raster layer. A layer containing the depth range specified for this research is obtained by applying a conditional expression of where the water depth is larger than -30 meter.

3.4.2 Radiometric correction and atmospheric correction

The WorldView-3 imagery is delivered in surface reflectance. Surface reflectance is typically thought of as a percentage, but was rescaled to values between 0 and 2047, representing 0 to 100% surface reflectance. Besides already being transformed from DN's to surface reflectance, the image is also atmospherically corrected using DigitalGlobe's AComp algorithm. The AComp algorithm uses the Aerosol Optical Depth (AOD), which is a measure of the amount of direct sunlight that is absorbed or scattered by particles in the atmosphere such as dust, smoke and pollution (DigitalGlobe, 2016). From pixel to pixel, the AOD and water vapor extent is estimated, and are integrated with the surface structures. The result is an atmospherically corrected image with minimized effects of haze, preserving the full spectral information.

3.4.3 Sunglint correction

To remove sunglint from imagery, Hedley et al. (2005) proposed a revised method on Hochberg et al. (2003). The original method assumes that in any given band, sunglint is linearly related to the brightness in the NIR band. However, in the original method only two isolated pixels are used to establish the relationship, whereas in the revised method, a sample of pixels are selected.

An areas is selected where sunglint is evident, but where spectral brightness underneath the pixels is expected to be homogenous. Therefore, areas containing sunglint in deep water are selected. From these areas, a linear regression is calculated for each separate band against the NIR band. In addition, the Coastal band was plotted against both NIR-1 and NIR-2 since experimental results from a research from Doxania et al. (2012) demonstrated a strong linear relationship between Coastal and NIR-2 as opposed to NIR-1. Finally to remove sunglint, the following equation is used:

$$R'_i = R_i - b_i(R_{\text{NIR}} - \text{Min}_{\text{NIR}})$$

Equation 1 (Hedley et al., 2005)

Where R_i is the pixel value in band i , b_i is the slope of the regression between band i and the NIR band, R_{NIR} is the pixel NIR value and Min_{NIR} is the minimal NIR value.

Before continuing to the next step, boats and waves are masked to further reduce the chance of classification errors. This is done by creating another mask with a conditional expression on the NIR band. By using visual comparison, the threshold value for NIR is decided where water (low NIR) is separated from other objects and waves (higher NIR).

3.4.4 Water column correction

The attenuation in the water column can be estimated with the measurement of surface reflectance of pixel samples selected at different depths for a homogeneous substrate, usually sand (Minghelli-Roman & Dupouy, 2014). Therefore, regions of interest (ROI) are clipped for each band from the raster image for further use. For each spectral band, surface reflectance can be plotted against depth. After these are plotted, the slope of the regression can be used as the proxy of the attenuation coefficient ratio for any substrate (Zoffoli et al., 2014).

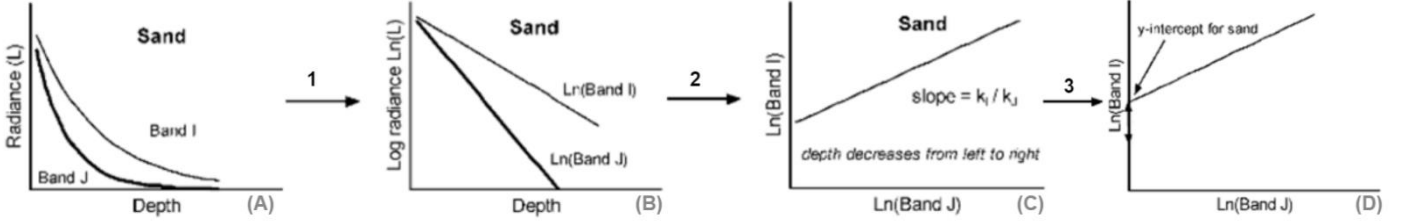


Figure 8 - Processes of water column correction (Green et al., 2000)

The steps that explain water column correction are shown in Figure 8. When water is clear, light will decay exponentially with increasing depth (A), meaning that when radiance is transformed using the natural logarithm, the relationship between radiance and depth becomes linear (B). This can be written as Equation 2.

$$X_i = \ln(L_i)$$

Equation 2 (Green et al., 2000)

When either the depth of the water at each pixel or other quantities are unknown, the ratio of the attenuation coefficients (k) can be used by creating a bi-plot of the log transformed radiance of two bands for one substrate at different depths (C). The attenuation coefficient is the severity of light attenuation in water for one spectral band. Since the effect of depth on the radiances has been linearised and the bottom type is constant, pixel values will follow a straight line according to their depth (Green et al., 2000).

To calculate the slope of the line a total last square regression is used instead of an ordinary least square regression. This uses the perpendicular distance to the regression line, making it inconsequential which band is chosen as the dependent variable (Keles & Altun, 2016). The raster's of the ROI are converted to points and exported to a table to calculate the variance of each band and the covariance between each pair of bands. Thereafter, the following equations are used to calculate the ratio of the attenuation coefficients.

$$\frac{k_i}{k_j} = a + \sqrt{a^2 + 1}$$

Where

$$a = \frac{\sigma_{ii} - \sigma_{jj}}{2\sigma_{ij}}$$

Equation 3 (Green et al., 2000)

Where σ_{ii} is the variance of band i , σ_{jj} is the variance of band j and σ_{ij} is the covariance of bands i and j .

Now each pixel value is converted to an index of bottom type, called the depth-invariant index using Equation 4. One depth-invariant index is calculated from a pair of spectral bands and this index can be used for further processing.

$$\text{Depth - Invariant Index}_{ij} = \ln(L_i) - \left[\left(\frac{k_i}{k_j}\right) * \ln(L_j)\right]$$

Equation 4 (Green et al., 2000)

3.5 Preparation in-situ data

Besides preprocessing of the satellite imagery, the in-situ data also has to be prepared before classification can take place. After visual interpretation of the imagery, it seems that some of the geolocations of field data points are wrong. The accuracy of the GPS drop point locations could be 5-10 meters. Therefore, the points that seem wrong will be removed. Besides, some classes are merged or removed based on the amount of samples in the classes.

3.6 Image classification

After pre-processing of the images and preparing the in-situ data, classification takes place. Figure 9 contains the general workflow that is followed when doing an image classification in ArcGIS Pro.

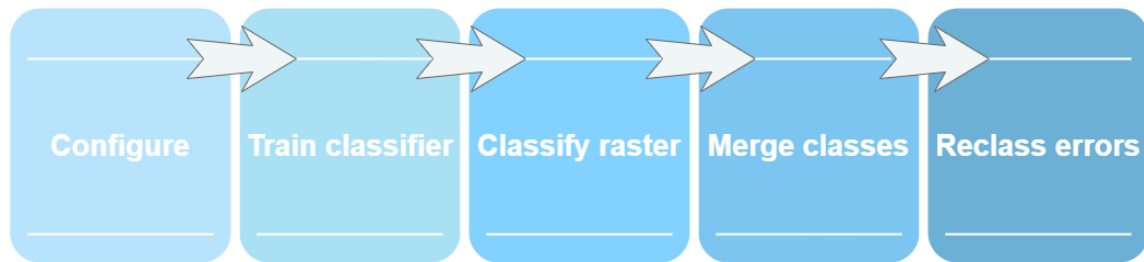


Figure 9 - General workflow supervised and unsupervised classification

The first step in classification is configure, where it is indicated which classification algorithm and type will be used in the classification. The second step is to train the classifier. For unsupervised classification, the number of classes is defined and other parameters for the algorithm to consider in the classifier are specified. For supervised classification, a subset of the ground truth points is used to train the algorithm. Two-third of the points is used for training and one-third of the points is set apart for validation of the algorithm later. Additionally in this step the classification scheme is provided, which is created from the training samples. The third step is where the actual raster is being created. After creating the raster, some classes might need to be merged. When using an unsupervised classification algorithm, this means that through visual inspection the classes are defined and merged while with supervised classification you get the option to combine subclasses from your classification scheme. Lastly, you can refine your results by reclassifying incorrectly identified classes before finishing and exporting the final classification.

This research includes the following image classification techniques:

3.6.1 Iterative Self-Organizing Data Analysis Technique (ISODATA)

The unsupervised classification technique that will be used is the iterative self-organizing data analysis technique (ISODATA). It is a technique that uses Euclidean distance to cluster elements into different classes, where the number of classes is assumed to be known. However, there is no spectral information about the classes available. The algorithm associates each pixel vector to one of the clusters based on the Euclidean distance from the pixel vector to each cluster centroid (Dhodhi et al., 1999). This is repeated till stopping criteria are reached which is either the number of classes or no cluster competent for split.

3.6.2 Maximum Likelihood Classifier (MLC)

The MLC is a well-known supervised classification approach that has been widely used in remote sensing applications (Hasan et al., 2012). Each unknown vector is assigned to the class that it has the highest probability of belonging to. Unlike other parametric algorithms, MLC takes both variance and covariance into account, resulting in better performance (Otukey & Blanschke, 2010).

3.6.3 Support Vector Machine (SVM)

SVM is a non-parametric machine-learning technique that is increasingly being used for benthic habitat mapping. It separates each pixel into classes with the use of boundaries or so-called hyperplanes (Wicaksono et al., 2019). SVM searches for the optimal separating hyperplane between classes (Ge et al., 2008).

3.6.4 K-Nearest Neighbor (K-NN)

The K-nearest neighbor assigns each object to a class by calculating the Euclidean distance between a point and each distance to its neighbors (Janowski et al., 2018). This algorithm uses a small number of training samples, making it easy to implement. The accuracy depends on the sample size and the distance between an unknown point and its nearest known sample (Mohamed et al., 2018). KNN has been applied much less often in marine habitat mapping studies, but it is recommended to be further explored based on previous researches (Janowski et al., 2018).

3.6.5 Random Trees (RT)

Random trees is an adaptation on the random forest algorithm by Breiman (2001). It is a classification algorithm that produces a construction of decision trees. Each tree is trained on a bootstrap sample, and from a random subset of all of the variables, the optimal variables are identified at each split (Degenhardt et al., 2017). Because of the use of multiple decision trees, overfitting of the model to the training dataset is avoided and therefore accurate predictions are usually made (Prajwala, 2015).

3.7 Accuracy assessment

Accuracy assessment or validation is a significant step in assessing the quality of the produced data. It indicates how each pixel is classified in comparison to their ground truth data. One-third of the ground truth data was held apart to create so called ‘accuracy assessment points’, containing one column with the groundtruth values and one column for the classified value. To compare class performance within a model, confusion matrices can be used. These summarize the classifier’s behaviour for every possible prediction-label combination (Opitz, 2022). From confusion matrices, the overall accuracy, user’s accuracy, producer’s accuracy and Cohen’s Kappa are derived. The overall accuracy is the ratio of correctly classified validation samples to the total number of validation samples per class (Zhang et al., 2013). It returns an overall measure of how much is correctly predicted over the entire data set and each unit is given the same weight and contribution to the value (Grandini et al., 2020). For benthic habitat mapping in shallow water, an accuracy of higher than 60% is usually accepted (Setlwan et al., 2022). Producer’s accuracy and user’s accuracy provide two different points of view on a map. Producer’s accuracy means how often ground truth features are shown correctly on the classified map while user’s accuracy means how often the classified value is actually represented in ground truth data. Lastly, kappa evaluates how well the classification algorithm performs compared to randomly assigned values. This value can range from -1 to 1, with negative values indicating a worse performance than random.

However, confusion matrices are not sufficient to compare the performance of two or more models (Pommé et al., 2022). There are many measures of classification accuracy to be used, reflecting on different aspects of the quality of a classification. There is however no perfect metric of classification accuracy (Foody, 2023). Widely used metrics are the Matthews correlation and the F1-score. The MCC is similar to kappa, where kappa tends to be more robust against classifier biases (Opitz, 2022). The F1-score is used in binary classification, but can also be used for multiclass classification in the form of the weighted F1-score (Equation 5). As with the F1-score, it uses precision and recall, but it averages each classes separate F1-score with their contributing weight :

$$\text{Weighted F1} = \sum_{i=1}^N W_i * \text{F1 Score}_i$$

Where

$$F1 = \frac{2 * TP}{2 * TP + FN + FP}$$

$$W_i = \frac{\text{No. of samples in class } i}{\text{Total number of samples}}$$

Equation 5 (Chicco & Jurman, 2020)

Where TP is true positive, TN is true negative, FN is false negative and FP is false positive. The magnitude of the weighted F1-score ranges from 0 to 1, with 0 representing a model unable to classify observation into a correct class and 1 being perfectly classifying observations in the correct class.

3.8 Additional analysis

After the preliminary results, some additional analysis is done to try to improve the accuracy of the water column corrected image. This includes comparison with the depth-invariant index of bands 1&3, alterations in training data and an object-based classification using a segmented raster.

3.8.1 Depth-Invariant Index bands coastal blue & green

As will be discussed in chapter 4.1.2, the Depth-Invariant Index of blue & green seemed to have the clearest results at first sight. To see if this is actually true, a classification is also performed on the Depth-Invariant Index of coastal blue & green for comparison.

3.8.2 Training data

Though some of the locations points were already adjusted based on visual inspection of the structures in the image, a new adjustment is made to the training data in hope of achieving higher accuracy. Since classification also depends on the number of training samples per habitat class, classes with a low amount of points are underrepresented. Instead of adding extra points for the class 'Algae, Seagrass & Sargassum', points are removed for classes 'Sand' and 'Coral & Gorgonian'. Hereafter, classification using this 'enhanced' dataset is compared to classification using the original dataset to see if there is a difference in performance.

3.8.3 Object-based classification

A segmented raster is created to see if object-based classification performs better than pixel-based classification. The process groups neighbouring pixels into objects that are similar in colour and shape characteristics. Certain levels of importance can be given to the spectral detail and the spatial detail and the minimum segment size has to be determined.

3.9 Comparison between 2009 and 2018

To compare change of benthic habitats over time a change detection can be performed. With the use of two thematic raster's, a change in pixel value for every location can be detected. Creating this change map is the easiest way to detect changes. However, for this research the imagery of 2009 was not useable for change comparison. Therefore, a visual inspection of changes is done.

4. Results

In this section, the results are given. First, the effect of the preprocessing steps is shown on the imagery, starting with sunglint removal and then water column correction. Then, results of five image classification algorithms are shown with its corresponding accuracies. Finally, additional results from further analysis are shown.

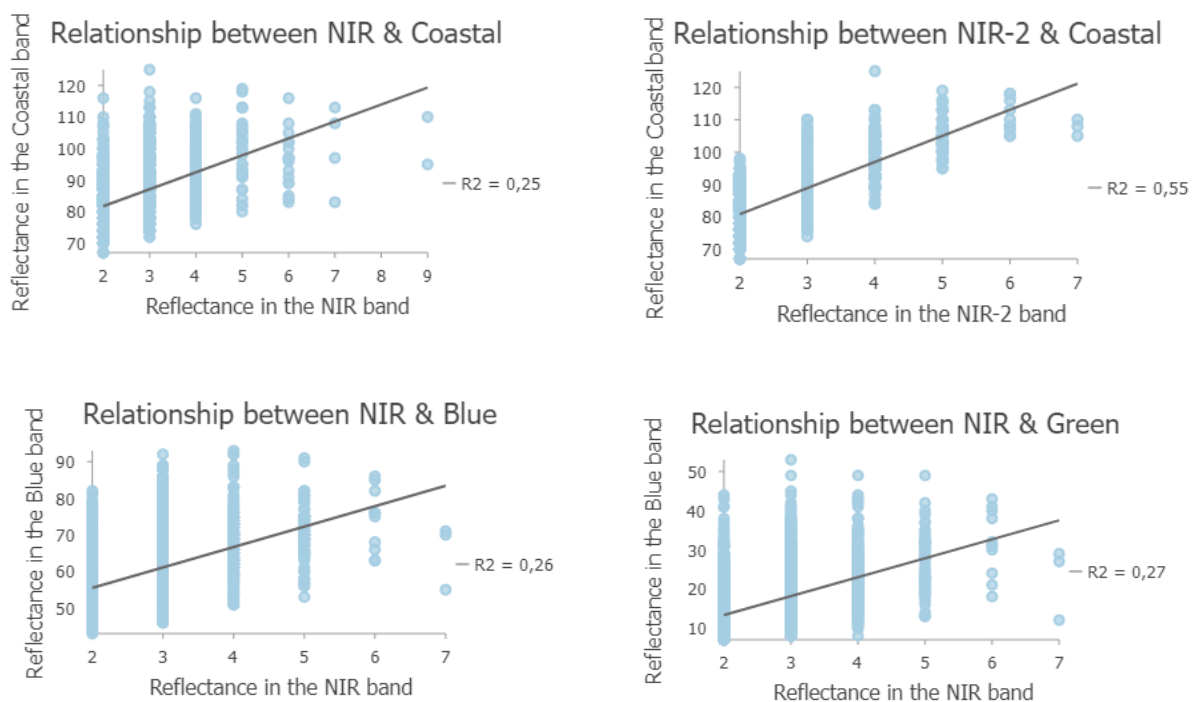
4.1 Preprocessing steps

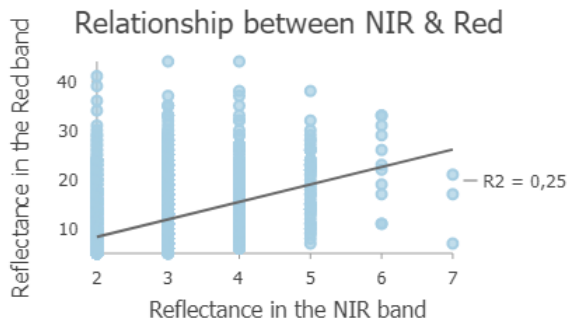
4.1.1 Sunglint removal

The first pre-processing step after masking out land and the areas that were deeper than 30 meters was sunglint correction. An area in the north-western part of the water around Statia was selected, where sunglint was most evident and where the water depth was larger than -30 meters (Figure 10). From this area, the relationship was established between the NIR band against the Coastal, Blue, Green and Red band. Furthermore, the relationship between NIR-2 and Coastal was also established. After analysing the bi-plots, two outlier pixels were removed from the selected area because of an exceptional high value in the NIR and NIR-2 band. The relationship between the bands and the slope that is used for Equation 1 are found in Figure 11. The minimum NIR value (Min_{NIR}) was obtained from the statistics of the NIR band and was 2 for this pixel sample.



Figure 10 - Areas selected for deglinting of the image. Source: DigitalGlobe. WorldView-3, ORTStandard2A level, 19 Nov, 2018.





Slope (b_i):

- NIR & coastal = 5.3779993786
- NIR2 & coastal = 8.071935135
- NIR & blue = 8.3592037082
- NIR & green = 7.6113660372
- NIR & red = 5.7842313856

Figure 11 - Bi-plots of areas selected for deglinting of pixel values of water penetrating bands against the NIR band and their slopes, reflectance is given in 11-bit pixel value

When comparing the deglinted Coastal band with the use of NIR-1 (Figure 12, left) and with NIR-2 (Figure 12, right), you see a slight difference in performance. In line with the results of the experimental research from Doxania et al. (2012), the right image shows less white speckle as seen in this example spot, but also in other parts of the images. Therefore, this corrected band is used for the band composite for further steps.

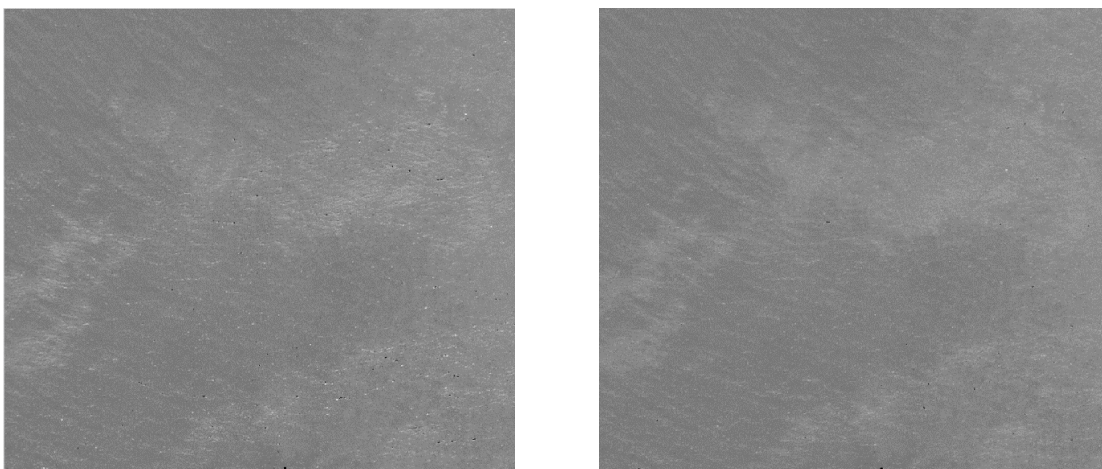


Figure 12 - Coastal band after sunglint removal using NIR-1 (left) and NIR-2 (right). Source: DigitalGlobe. WorldView-3, ORTStandard2A level, 19 Nov, 2018.

After sunglint removal, waves and boats are masked by using a threshold value for the NIR band of 15, chosen after visual inspection of the image. In Figure 13, a composite of the same area is depicted before (left) and after (right) sunglint removal. As it can be observed, there is some visual improvement in the images. However, after using an unsupervised classification technique to see the effect, it showed little variation in the deeper water as opposed to the image before sunglint removal. (Appendix A). Therefore, the image before sunglint is used for further processing.

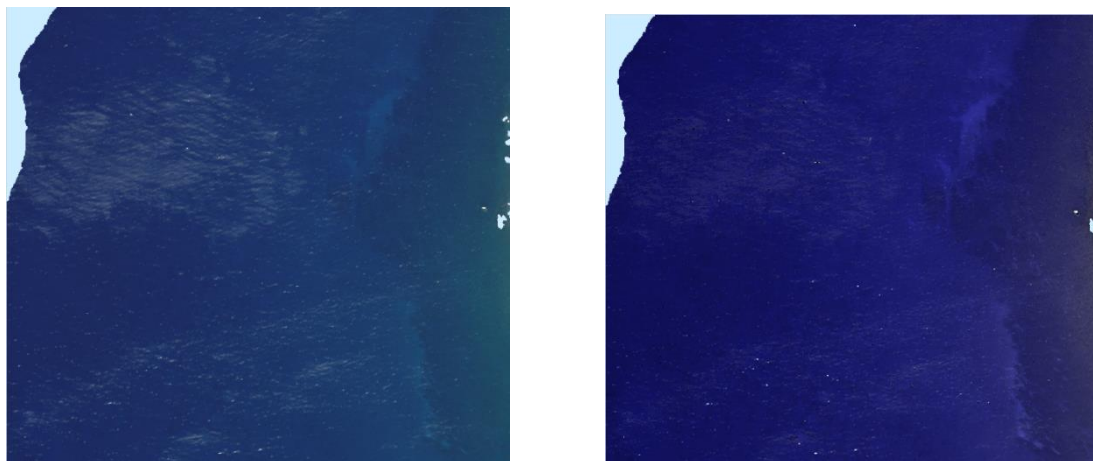


Figure 13 - Results before (left) and after (right) sunglint removal. Source: DigitalGlobe. WorldView-3, ORTStandard2A level, 19 Nov, 2018.

4.1.2 Water column correction

The water column correction was applied to the original image without sunglint removal. To start, areas of various depth were selected, where the bottom type was sand. First each separate band is transformed using the natural logarithm. Then the variance for each separate band is calculated and the covariance is calculated for each pair of bands (Table 2) to use for the calculation of the attenuation coefficient (Equation 3).

Table 2 - Parameters used for performing water column correction

Variance of band		Band ratios				
		1/3	2/3	3/5	1/5	2/5
1 coastal	0.01785147					
2 blue	0.04063345					
3 green	0.44885774					
5 red	0.33762298					
Covariance		0.0074059	0.0190319	0.0211680	0.0015286	0.0054999
a		-29.0987100	-10.72474	2.627427	-104.59370	-26.99954
Ki/Kj		0.0171778	0.04652029	5.4387110	0.0047803	0.01851249

The Depth-Invariant Indices (DII) were calculated using Equation 4. From the DIIs, an RGB image and an RGC image were created. Since DIIs containing the red band showed striping after unsupervised classification (Appendix B), both RGB and RGC were eliminated for the following steps. As seen in other research (Contreras-Silva et al., 2012), classification can also be performed on one depth-invariant index image of two bands. Since the blue-green DII gave the clearest image, this DII was initially used for comparison of the classification algorithms.

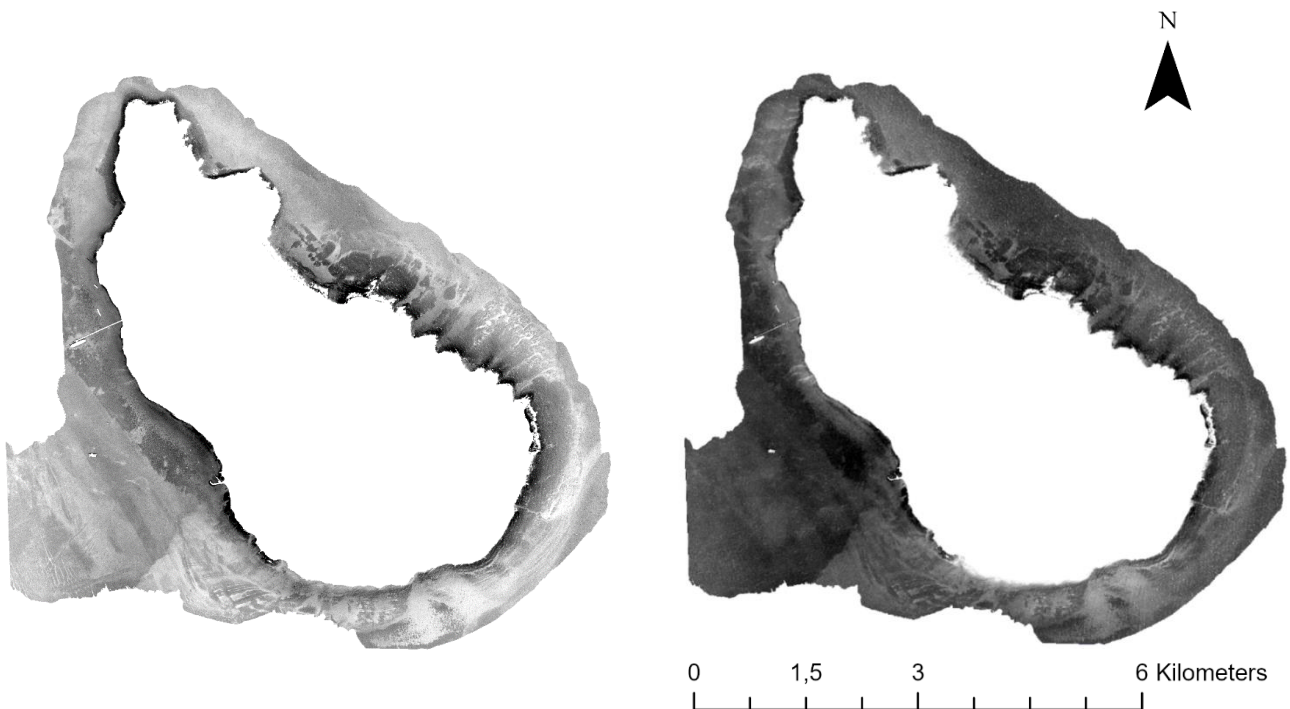


Figure 14 – Depth-Invariant Index of bands 2 and 3 compared to Depth-Invariant Index of bands 1 and 3. Source: DigitalGlobe. WorldView-3, ORTStandard2A level, 19 Nov, 2018.

4.2 Image classification

The image classification is performed on the multispectral image before preprocessing steps and on the DII of bands 2 and 3 (from now on referred to as MS and DII_23) to analyse the effect of the water column correction. For both MS and DII_23, results were often speckled. Therefore, for each classification method the original image, a 3x3 smoothed image and a 5x5 smoothed image were compared. Only the classification with the highest accuracy for each is included in this report.

After analysing the field data points and performing the first classification, the benthic habitat classes were redefined. Rubble only has 18 observations, making it hard to identify this class from the imagery. Due to spectral similarity of Sargassum, Algae & Seagrass (Tamondong & Blanco, 2017), these classes were merged. Also, Gorgonian and Coral were merged. The classes used for classifying are the following: (1) Sand, (2) Coral & Gorgonian and (3) Algae, Sargassum & Seagrass

4.2.1 Iterative self-organizing data analysis technique (ISODATA)

The initial result of an ISODATA classification is a classification with unassigned classes (Figure 15, left side). In the MS classified image (Figure 15, top), the classes seem to consist of rings around the island from shallow towards deeper water. In the DII_23 image, the classes are more distributed over the range of depths. After assigning classes and performing an accuracy assessment, the accuracy for the images were 40.5% and 39.2% respectively (Table 3).

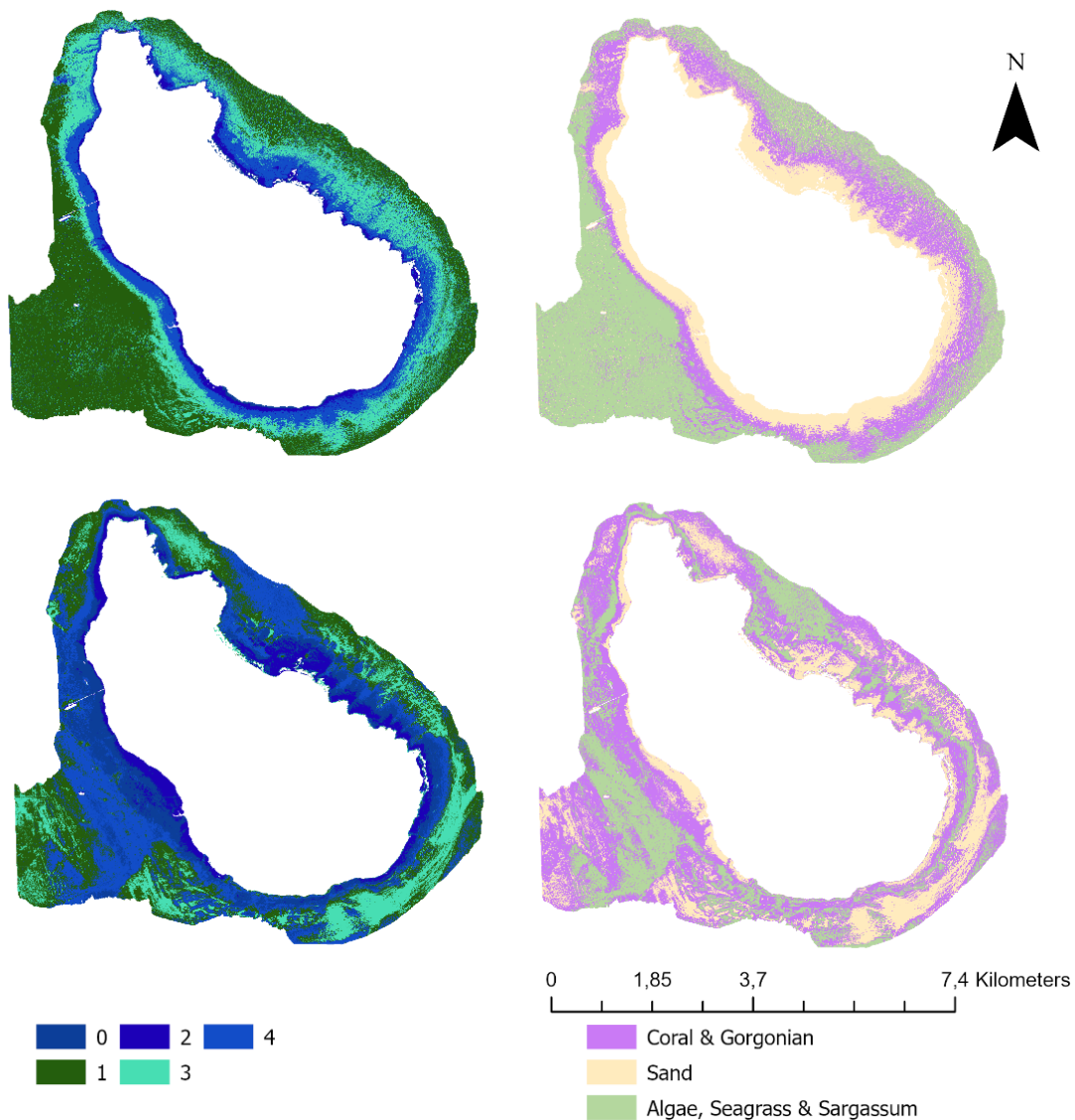


Figure 15 - Results of unsupervised classification ISODATA on MS (top) and DII_23 (bottom)

To test whether the result is truly because of the water column correction and not because of the water penetrating properties of the blue band that is used in the DII, an ISODATA classification is also performed on the singular blue band (Figure 16). The results of the comparison show that DII_23 has more structures and variation in the deeper parts of the water, especially in the south-western part of the water.

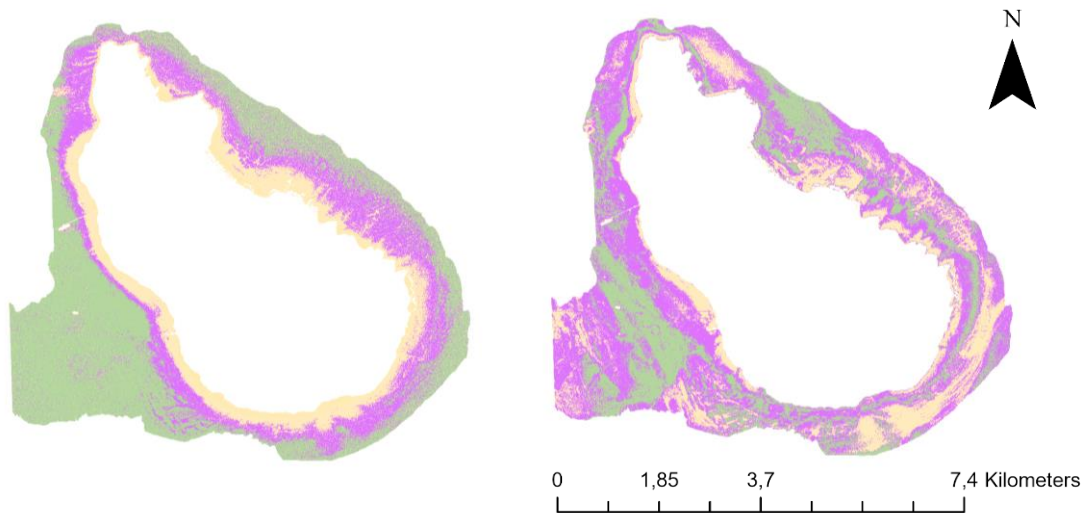


Figure 16 - Results ISODATA on blue band (left) compared to DII_23 (right) (see Fig 15 for legend)

4.2.2 Maximum Likelihood Classifier (MLC)

The maximum likelihood classifier is the first supervised classifications method that is shown with the use of training data. It has a smooth outcome for both MS and DII_23, but the distribution of the classes differ significantly. In the MS image, the south-eastern side consists of mainly coral, while the DII_23 image consists mainly of sand. This difference can also be seen in the accuracy of both classifications, where MS has an accuracy of 56.9%, while DII_23 has an accuracy of 33.3%.

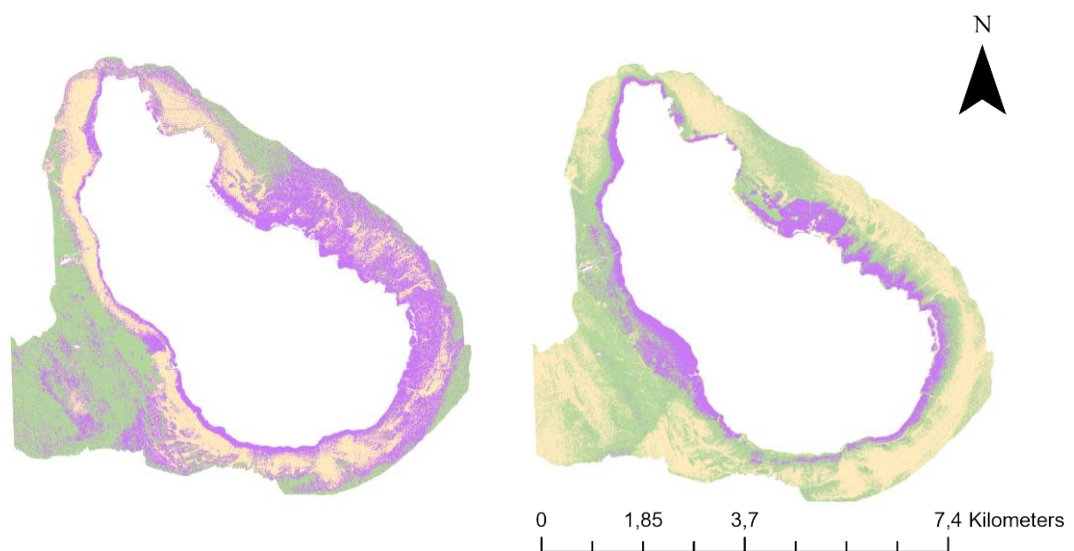


Figure 17 - Results MLC on MS (left) and DII_23 (right) (see Fig 15 for legend)

4.2.3 K-Nearest Neighbor (K-NN)

The K-Nearest Neighbor classifier results in a large area covered by coral & gorgonian in both images. A notable difference between the two results is how the DII_23 image is very speckled, while the MS image is more smoothed with more compact areas. The non-smoothed DII_23 image showed a higher accuracy (44.4%) in comparison with the 5x5 smoothed image (35.3%) and is therefore depicted here. Again, MS showed to have a higher overall accuracy (65.4%) in comparison with DII_23 (44.4%).

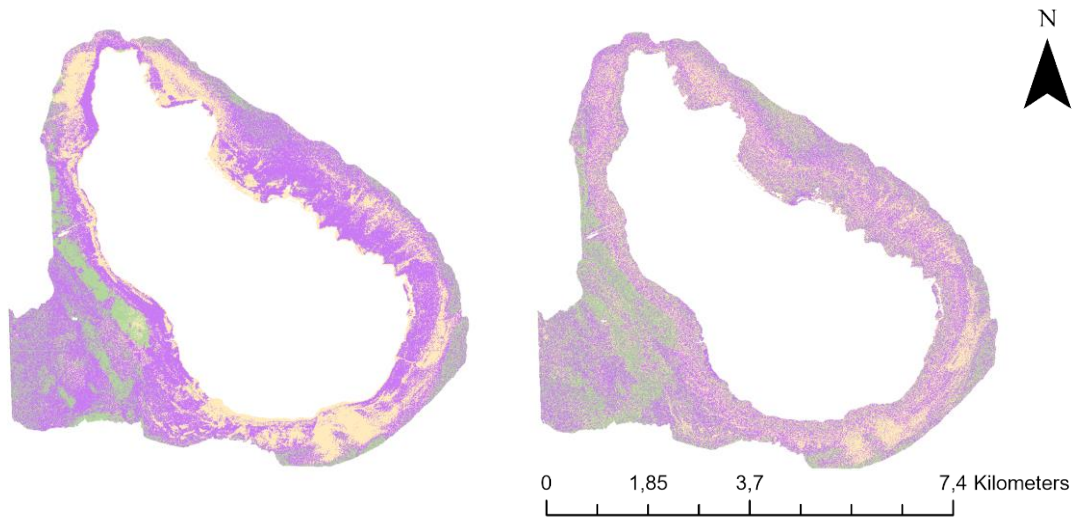


Figure 18 - Results K-NN on MS (left) and DII_23 (right) (see Fig 15 for legend)

4.2.4 Support Vector Machine (SVM)

The support vector machine results in a classified image where each class is well represented. In the MS image more area is classified as coral & gorgonian, while in the DII_23 image there is more area classified as sand. The image after water column correction again shows more variation in the deeper areas of the water but also again has a lower accuracy than the MS image (41.2% and 62.7% respectively).

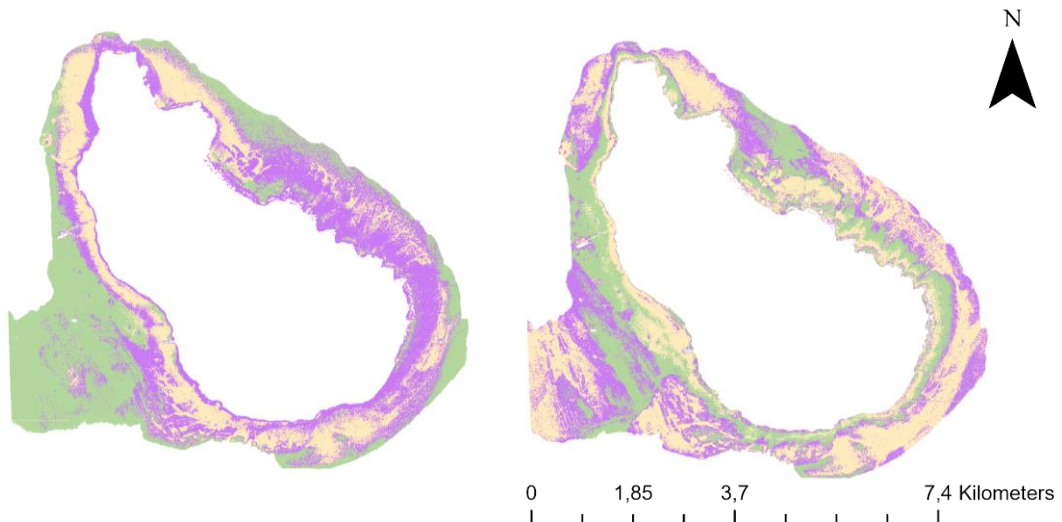


Figure 19 - Results SVM on MS (left) and DII_23 (right) (see Fig 15 for legend)

4.2.5 Random Tree (RT)

The last classifier that is tested in this research is the Random Trees. 5x5 smoothing resulted in the highest accuracy for both MS and DII_23. There is however, a notable difference in how smooth the outcome is. The MS image has smoother and larger areas, while the DII_23 image is a lot more speckled. The accuracy for MS is 67.3% and DII_23 resulted in a lower accuracy of 38.6%.

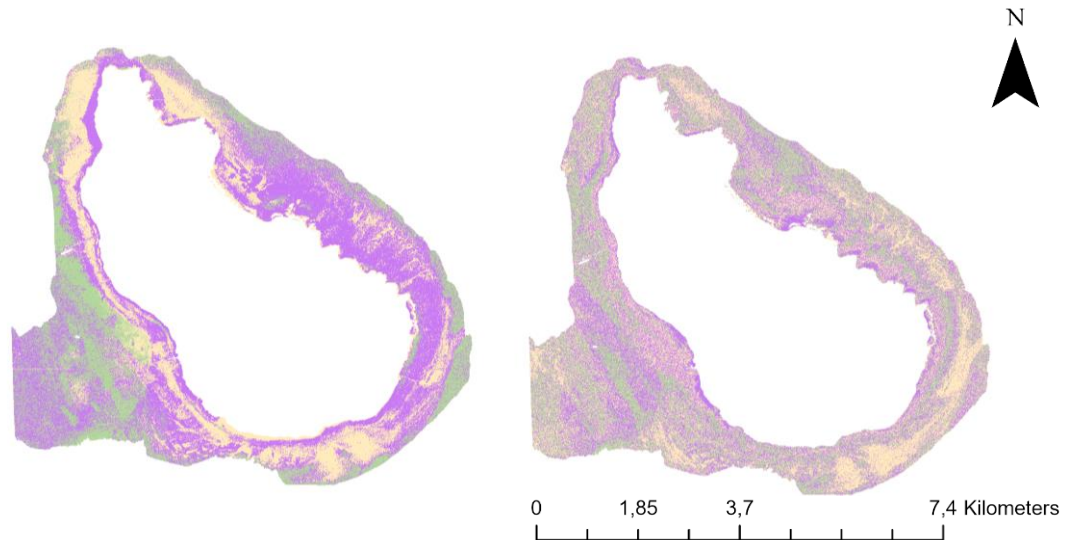


Figure 20 - Results RT on MS (left) and DII_23 (right) (see Fig 15 for legend)

4.3 Accuracy assessment

The accuracy of each of the classified maps is calculated with the use of a confusion matrix. A summary is presented in Table 3 containing the overall accuracy (%) and the user's accuracy per class (%) for each of the classifiers. As already discussed in section 4.2, the accuracy of the multispectral image is higher compared to the water column corrected image in all of the classifiers. Overall, the class 'Coral & Gorgonian' achieved the highest user's accuracy for each of the classifiers, often followed by 'Sand' and finally 'Algae, Seagrass and Sargassum'.

Table 3 - Overall accuracies and User's accuracy per class for five classification algorithms

		Overall accuracy (%)	User's accuracy per class (%)		
			Coral & Gorgonian	Sand	Algae, Seagrass & Sargassum
ISODATA	MS	40.5	52	31.3	36.6
	DII_23_5x5	39.2	49.4	34.8	24.5
MLC	MS_3x3	56.9	68.3	59.1	39.1
	DII_23	33.3	53.8	36.5	24
K-NN	MS_5x5	65.4	69.6	64.9	50
	DII_23	44.4	54.3	31.3	35
SVM	MS_5x5	62.7	72.6	66.7	55.6
	DII_23_5x5	41.2	56.5	43.1	24.5
RT	MS_5x5	67.3	78.6	65.2	43.1
	DII_23_5x5	38.6	45.6	40.8	25.6

	ISODATA		MLC		K-NN		SVM		RT	
	MS	DII_23	MS	DII_23	MS	DII_23	MS	DII_23	MS	DII_23
Weighted F1-score	0.3864	0.3871	0.5754	0.3189	0.6435	0.4388	0.6348	0.4147	0.6701	0.3890
Kappa	0.1233	0.0189	0.3319	0.0707	0.4126	0.0965	0.4347	0.1264	0.4627	0.0507

Table 4 - Calculated metrics for five classifiers

The classification algorithm that resulted in the highest accuracy for the multispectral image is the Random Trees classifier, followed by K-Nearest Neighbor. The classifier that had the highest accuracy for DII_23 is K-Nearest Neighbor followed by Support Vector Machine. SVM, K-NN and RT have similar accuracies, but SVM looks the smoothest visually for the water column corrected image and represents each of the classes most evenly.

When looking at the metrics that are calculated for each classifier, again Random Trees scores highest for MS on both metrics closely followed by K-Nearest Neighbor and Support Vector Machine. For DII_23, K-Nearest Neighbor scores highest on the weighted F1-score, followed by Support Vector Machine. SVM has the highest value for kappa, followed by K-NN. It is worth noting that the kappa value for each of the classifiers on image DII_23 is very low in comparison with the multispectral image.

4.4 Additional analysis

As discussed in the methodology, some addition analysis is performed to see if it helped to increase accuracy of the water column corrected image. It is decided only to continue with the Support Vector Machine algorithm, based on the previous results.

4.4.1 Depth-Invariant Index bands coastal blue and green

Depicted here is a comparison between DII_13 (Figure 21, left) and DII_23 (Figure 21, right). There is a clear visual difference between the two classified images. The right image again shows more variation in the deeper parts of the water and more alternations of habitat. However, when looking at the information in the confusion matrix (Table 5), DII_13 has a better performance regarding classification of habitats. Therefore, other additional analysis steps are performed on DII_13.

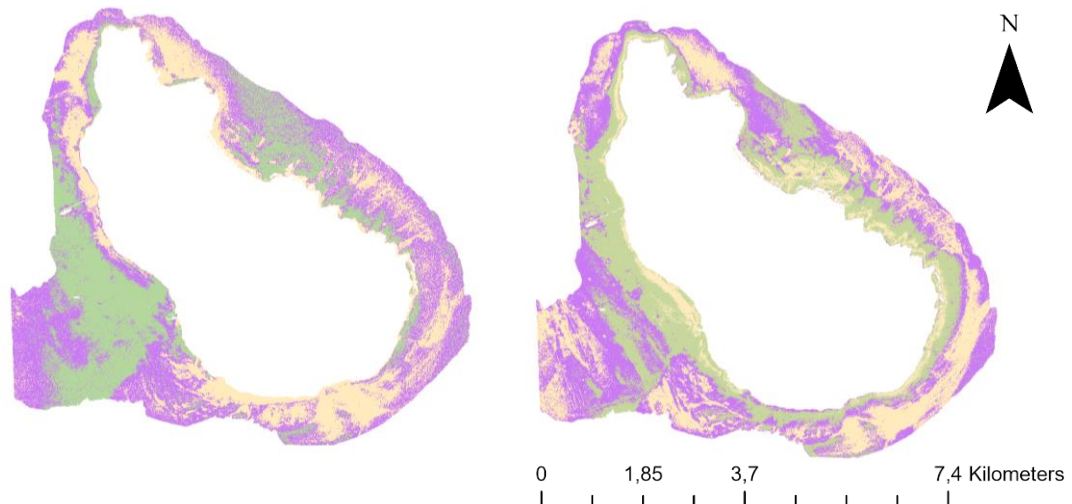


Figure 21 - SVM classification for DII 13 and DII 23 (see Fig 15 for legend)

Table 5 - Overall accuracies and accuracy per class for DII_13 and DII_23

	Overall accuracy (%)	User's accuracy per class (%)		
		Coral & Gorgonian	Sand	Algae, Seagrass & Sargassum
DII_13_5x5	55.6	67.1	50	41.5
DII_23_5x5	41.2	56.5	43.1	24.5
MS_5x5	62.7	72.6	66.7	55.6

4.4.2 Training data

Before the start of all image classification, the in situ data was already altered by adding extra points for the class 'Algae, Seagrass & Sargassum' and by removing points that seemed to be in an incorrect location. In this step, no extra points were added for Algae, Seagrass & Sargassum because they can not be verified from ground truth data. Instead, to create a more even distribution, points are removed for the classes coral and sand to remove some of the bias.

Table 6 - Number of samples and percentage of pixels before (left) and after (right) training data removal

	# samples	Pixels (%)
Coral & Gorgonian	131	36.09
Sand	147	40.30
Algae, Seagrass & Sargassum	84	23.61

	# samples	Pixels (%)
Coral & Gorgonian	109	32.11
Sand	111	36.53
Algae, Seagrass & Sargassum	84	31.36

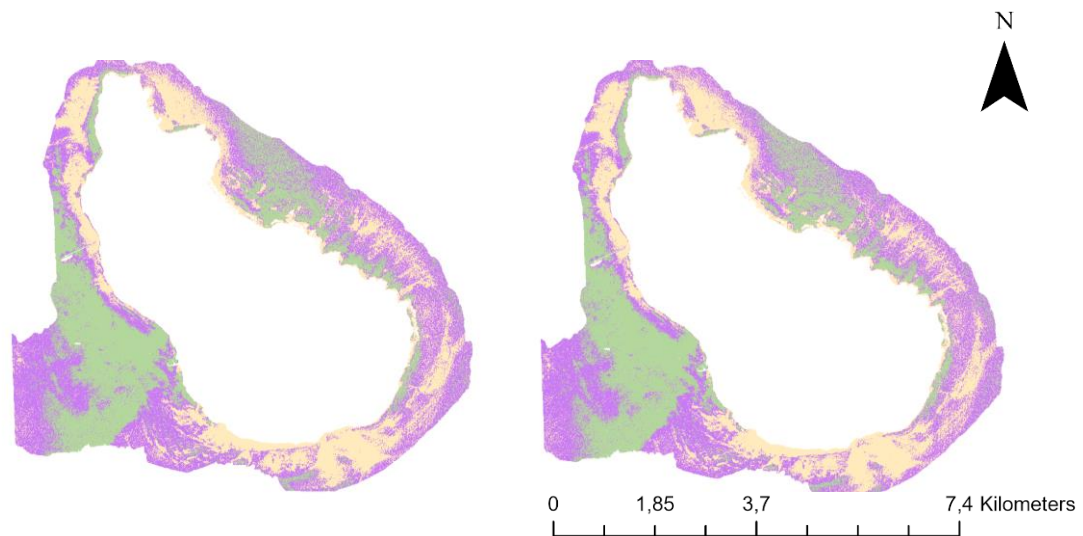


Figure 22 - SVM classification with 'original' training data (left) and with 'enhanced' training data (right) (see Fig 15 for legend)

The results of altering the training data is shown in Figure 22. There is almost no visual difference between the classification with the enhanced training data and original training data. However, there is a slight improvement in accuracy from 55.6% to 56.7% as seen in Table 7.

Table 7 - Accuracy assessment SVM before and after altering training data

	Overall accuracy (%)	User's accuracy per class (%)		
		Coral & Gorgonian	Sand	Algae, Seagrass & Sargassum
DII_13_5x5 – Original training data	55.6	67.1	50	41.5
DII_13_5x5 – Enhanced training data	56.7	60	64	44.4

4.4.3 Object-based classification

A segmented raster (Figure 23) is created to group pixels into objects. The results of the classification with use of a segmented raster gives a very smooth output because of the use of objects rather than pixels. However, 'Algae, Seagrass & Sargassum' seems very underrepresented in the resulting raster. The accuracy of this object-based classification is however similar to the pixel-based classification.

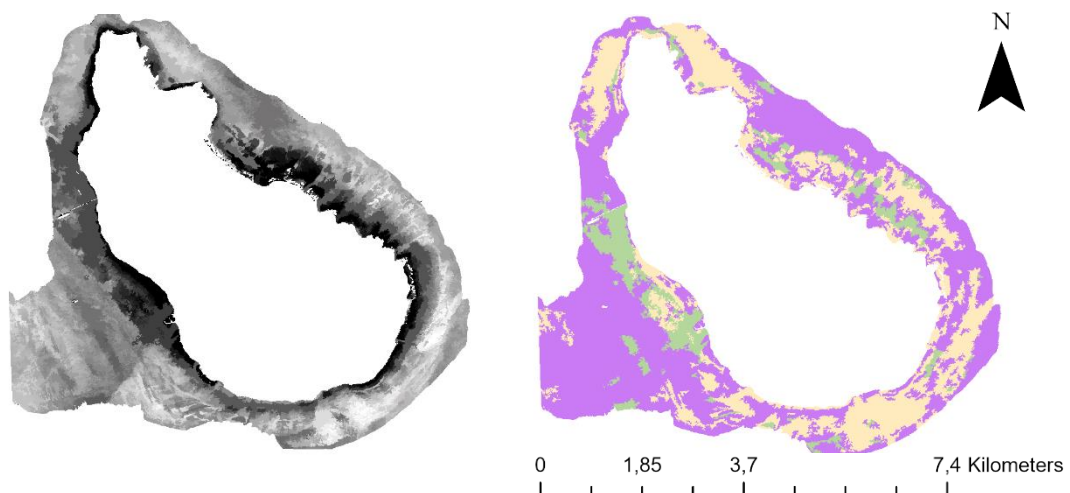


Figure 23 - Segmented raster (left) and SVM object-based classification (right) on DII_13 (see Fig 15 for legend)

Table 8 - Accuracy assessment SVM object-based classification

	Overall accuracy (%)	User's accuracy per class (%)		
		Coral & Gorgonian	Sand	Algae, Seagrass & Sargassum
DII_13 - segmented	56	56.5	61	41.2

4.5 Comparison between 2009 and 2018

To compare the satellite imagery from 2009 and 2018, the image from 2009 had to be corrected similarly to the image of 2018. As can be seen in the left of Figure 24, the original imagery is slightly cut off in the north and had some clouds and cloud shadows in the area of interest. These were masked out as well as deep water, land, waves and boats (Figure 24, right).

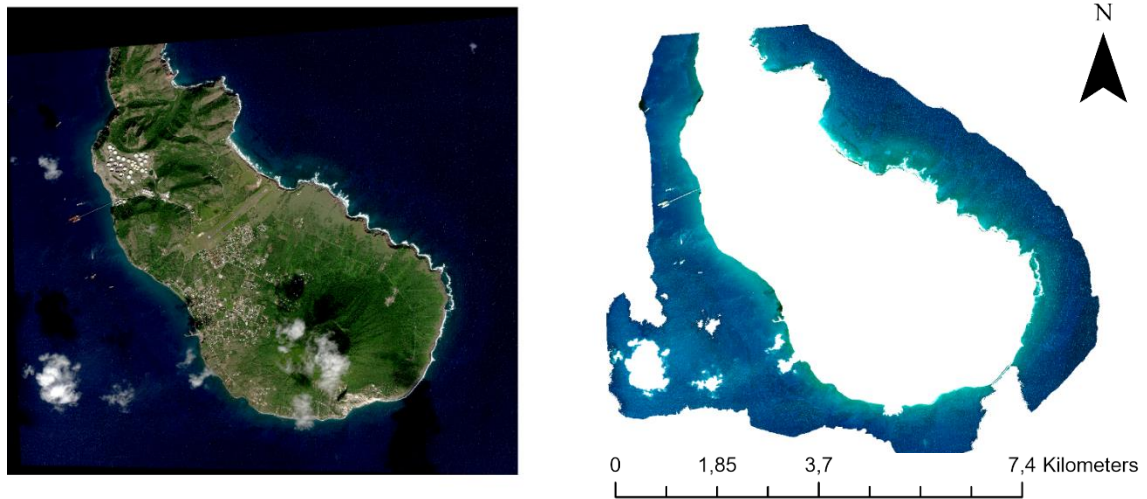


Figure 24 - Original satellite imagery (left) and after clipping (right). Source: DigitalGlobe. WorldView-2, ORTStandard2A level, 6 Dec, 2009.

After masking, sunglint removal was performed, which resulted in more contrast and better visibility (Figure 25). However, because of the large amount of small waves that were still apparent, the resulting classification was very speckled (Appendix C). Therefore, an accurate change detection on classified rasters can not be performed. When habitat types are known, judgments can be made by an expert on changes in structure. Therefore the visible structures of both years are shown in Figure 26.

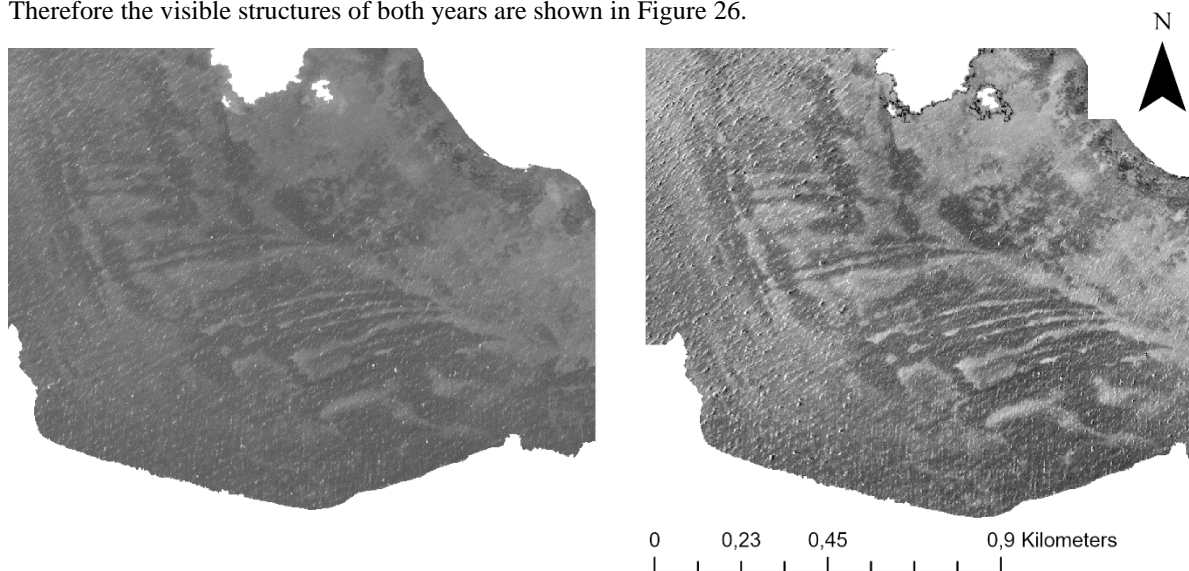
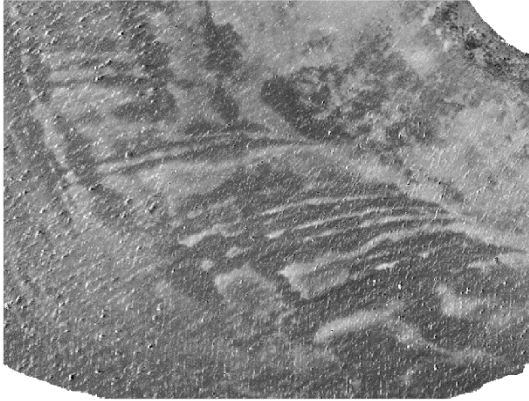


Figure 25 – Structure in the water shown in the blue band of 2009 imagery before (left) and after (right) sunglint removal. Source: DigitalGlobe. WorldView-2, ORTStandard2A level, 6 Dec, 2009.

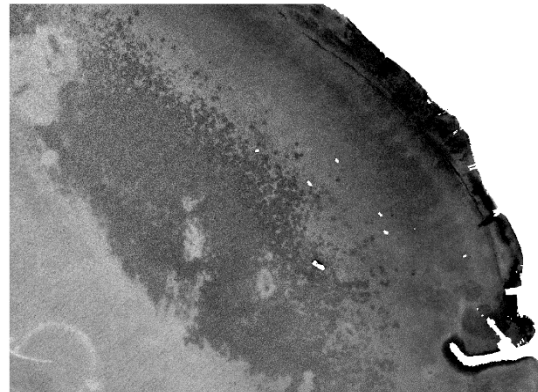
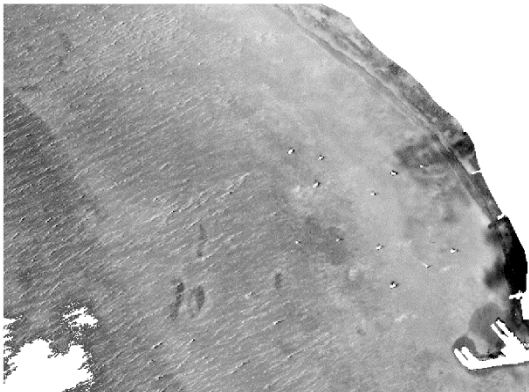
Structures found in 2009

Structures found in 2018

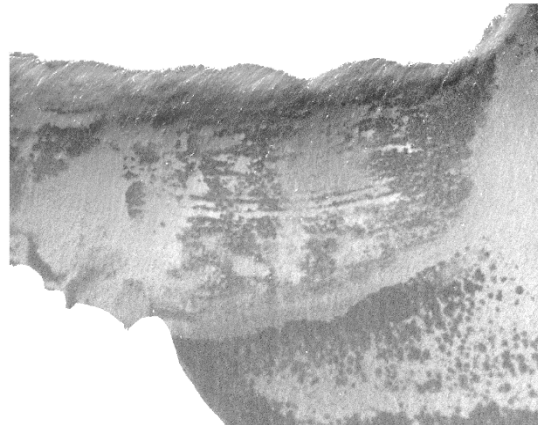
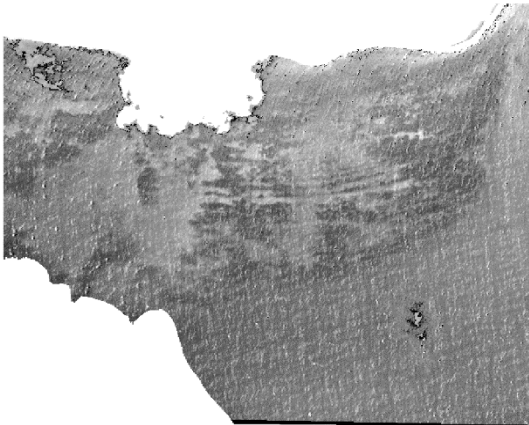
(A)



(B)



(C)



(D)

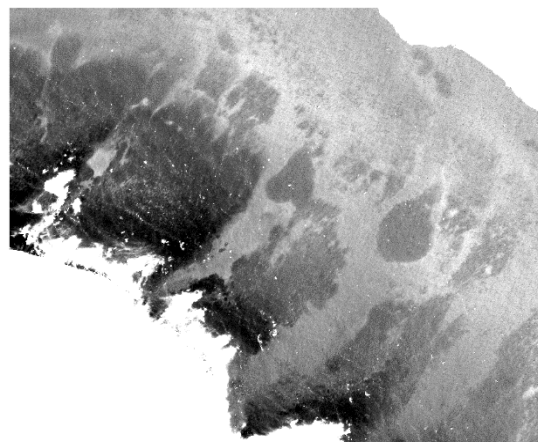
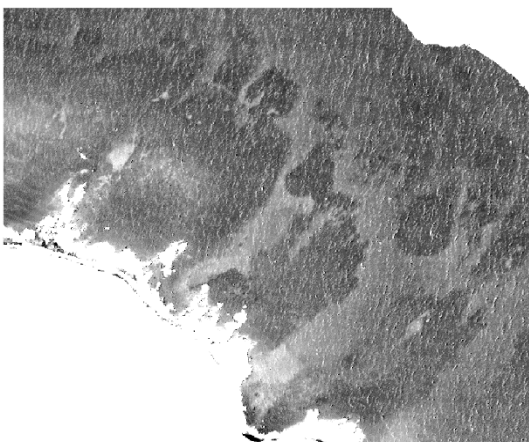


Figure 26 – Comparison of four apparent structures (A,B,C,D) found in the same locations in 2009 and 2018.

5. Discussion

In this chapter the characteristics of the data and the performance of the preprocessing steps will be discussed. The influence of the preprocessing steps on the imagery will be elaborated on and the different classification algorithms are compared.

5.1 Characteristics of the data

The quality of the satellite imagery is of great importance for analysis. The imagery used in this research was delivered with an ACOMP radiometric correction that is performed by DigitalGlobe, resulting in a clear image to begin with, with no clouds and almost no influence of waves. It therefore can be noted that the original image was already of high quality.

A limitation in this research was the ground truth data that was provided. The field data did not cover the entire research area with gaps in the north-eastern part of the island and the western part of the island. Also no samples were collected between 0 and -5 meter, eliminating the more shallow benthic data. Lastly, the points were not representative of all of the habitat types. Some classes had a high amount of points while other had very few. Uneven training distribution can contribute to a classification algorithm's performance (Wicaksono & Aryaguna, 2020). Therefore it is recommended to obtain an even distribution of training samples for each class. The habitat types with very few points could therefore not be recognized by the machine learning algorithms and were either removed or merged to other benthic habitats. Also, combining classes from the classification scheme can influence the separability between classes due to mixing of statistics (Wicaksono & Aryaguna, 2020).

5.2 Preprocessing steps

5.2.1 Sunlint removal

After removal of land and deep water from the image, the first preprocessing step that was performed is sunlint removal. The imagery had low amounts of sunlint to begin with, only in the north-western part of the image. After performing sunlint removal these small areas of sunlint were visually removed. However, after an ISODATA unsupervised classification (Appendix A), although some of the sunlint seems reduced, there was little variation in the deeper water left as compared to before sunlint removal. In Figure 27 the mean spectral profile is shown from an area containing sunlint and an area that does not contain sunlint both before and after performing sunlint removal. The area that does not contain sunlint follows almost exactly the same profile before and after performing sunlint removal. However, the areas that contained sunlint has a lower reflectance value after sunlint removal, as expected. When looking at the classified image before and after sunlint removal in Appendix A, the areas where sunlint is evident are classified as sand, which is in line with the field data points. Therefore, it could be that there was too little sunlint evident in the image to benefit from sunlint removal.

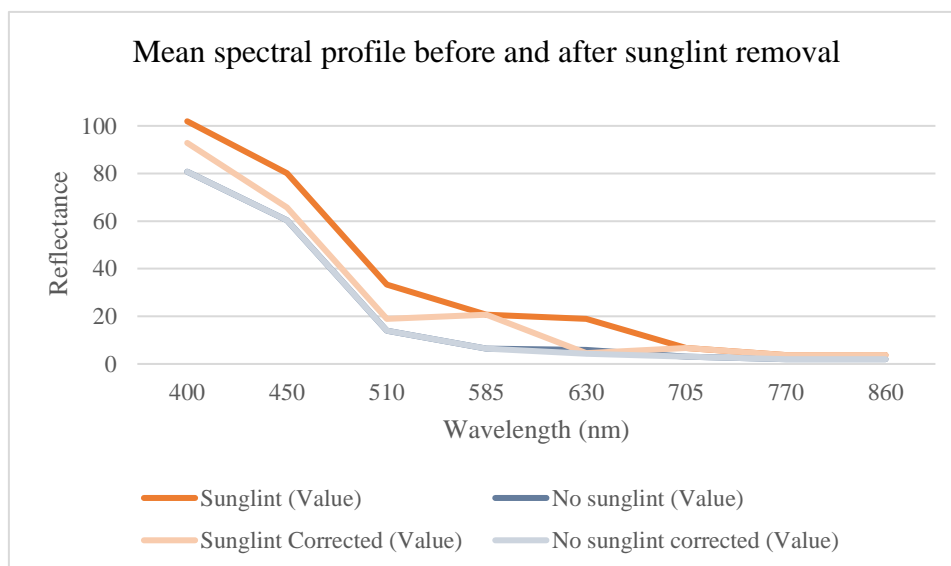


Figure 27 - Mean spectral profile before and after sunlint removal

5.2.2 Water column correction

As already mentioned before, WorldView-3 has an additional spectral band called coastal blue with a wavelength of 400-450 nm. Attenuation in the water column is theoretically least for this band since it has shorter wavelengths than other water penetrating bands. However, it is absorbed by chlorophyll in vegetation and is influenced by atmospheric scattering more than longer wavelengths, which could negatively influence the signal (Mandlbürger et al., 2018). Also, when looking at Figure 28, you can see that spectral separability between classes coral and seagrass should be very similar for the coastal band and the blue band.

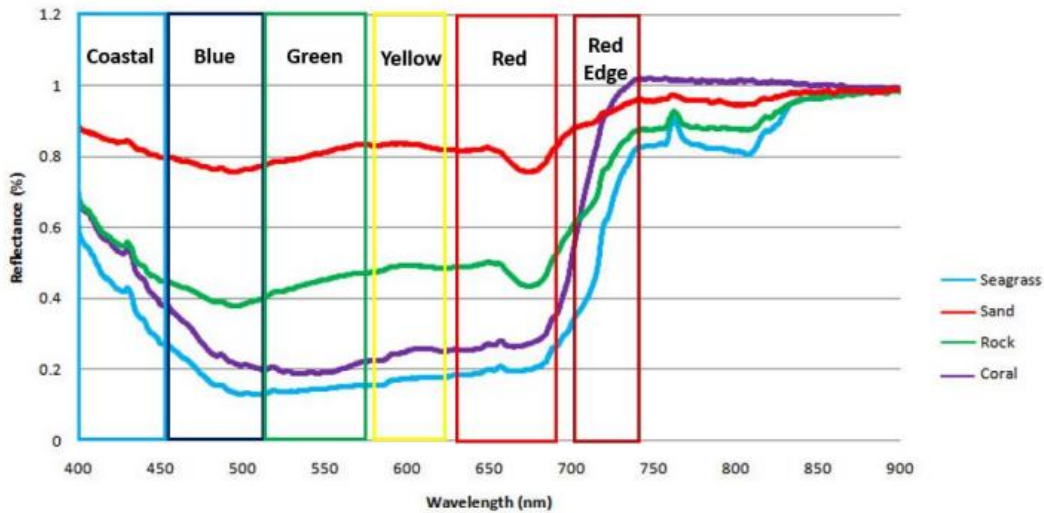


Figure 28 - Comparison of underwater reflectance values of different benthic covers with the corresponding band (Tamondong & Blanco, 2017)

In this research the coastal band is compared with the blue band during the water column correction. The water column corrected image that was initially used for classification was the DII_23. This was based on the visibility of structures in the deeper part of the water. In Figure 29 some structures that are clearly visible in deep water from DII_23 are presented with the classified rasters MS, DII_13 and DII_23 to compare how the three raster perform.

As seen in this Figure, the structures seen in deep water are best identified from DII_23. However, as shown in Table 5 in the results section, the accuracy of the multispectral classified raster remains higher than both DII_23 and DII_13. Since the water column corrected image uses the values of one singular band, this limits the separation of habitat spectra to one dimension (Green et al., 2000). This could potentially result in lower accuracies for the water column corrected images. Another research on WorldView 2 and 3 imagery on depths up till 35 meter also concluded that water column correction did not improve the results (Mederos-Barrera et al., 2022). It is said to be dependent on the turbidity of water, how homogenous the optical properties are both vertically and horizontally and on the water depth.

Although structures do not become more clear with use of the coastal blue band in comparison with the blue band, accuracies are higher after classification. DII_23 had an accuracy of 41.2% while DII_13 had an accuracy of 55.6%. Although the coastal band did not result in a higher accuracy, having an additional water penetrating band does increase potential combinations for identifying optimal band ratios which can be used for example for depth estimation (Mandlbürger et al., 2018).

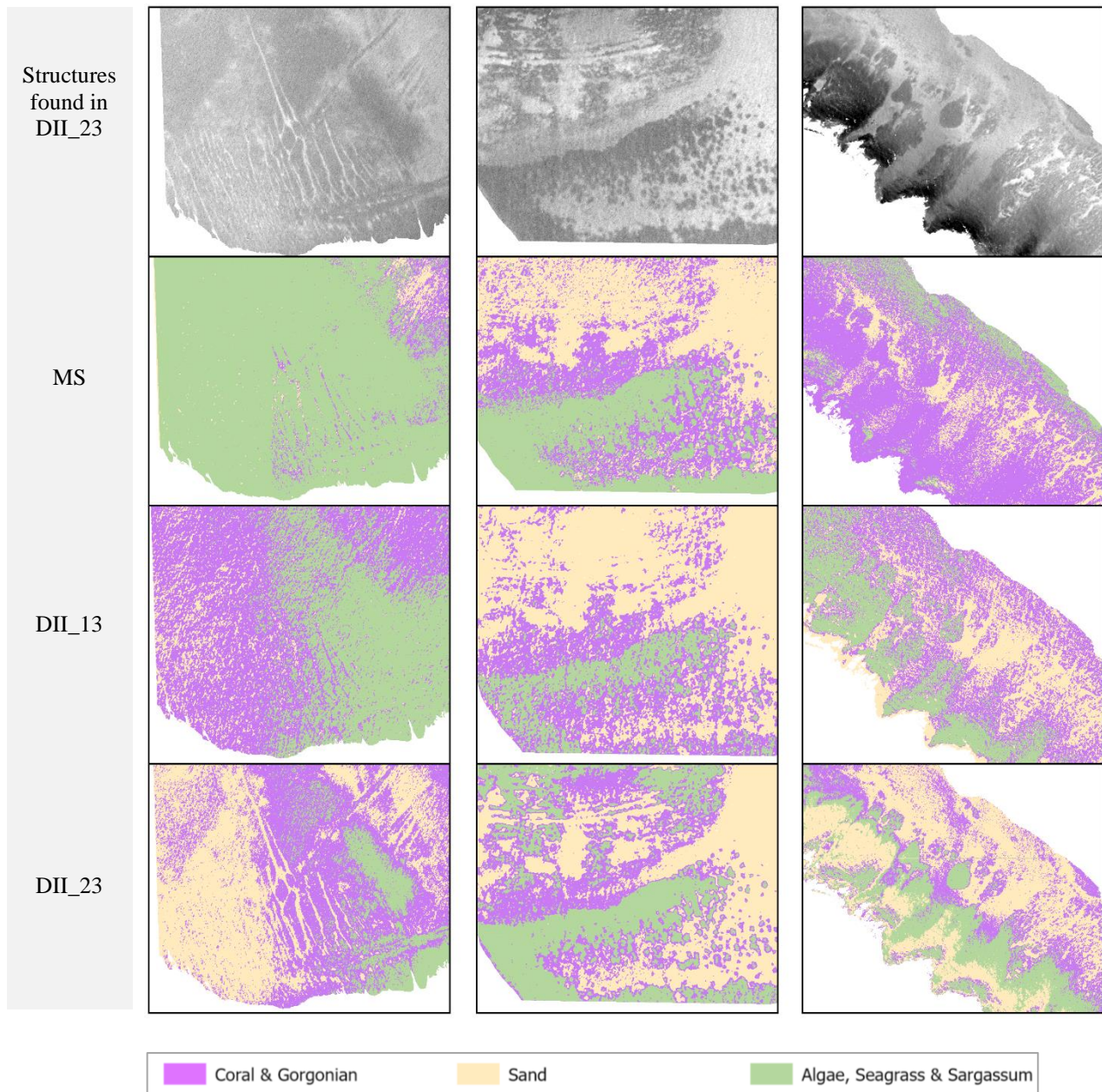


Figure 29 - Comparison of SVM classification of the apparent structures on MS (top), DII_13 (middle), DII_23 (bottom)

5.3 Classification algorithms

The aim of this research was to classify the benthic habitats around St. Eustatius. In literature many classification algorithms have been tested, with different findings. Therefore, for this research a comparison was made with unsupervised and supervised classification algorithms.

First an unsupervised classification was performed on the original imagery prior to preprocessing. From this classification some structures in the water could already be seen (Appendix A). After separating the area into segments, the most common method to assign a habitat is from ground-truth observations. It should be noted that although it is called unsupervised classification, prior knowledge of the data is beneficial to define a number of classes (Calvert et al., 2015).

In similar research, varying levels of success have been reported from unsupervised classification (Calvert et al., 2015). Although unsupervised classification resulted in the lowest accuracies, it could be a great tool to use prior to ground truth surveying to have a first idea of the benthic surface as the location, size and concentration of habitat types can already be identified (Green et al., 2000). This was especially true when looking at the water column corrected image (Fig 15, bottom). From this classification, most of the structures were visible. Green et al. (2000) also mentions that habitat maps produced using unsupervised classification can be significantly improved by image processing such as water column correction.

When comparing the supervised classification algorithms, accuracies were relatively similar between some classifiers. The Maximum Likelihood Classifier scored lowest on the accuracy assessment for both MS and DII_23. The other three classifiers, RT, SVM and K-NN had similar accuracies, with only ~3-5% differences. This slight difference is also seen in the calculated metrics, where the weighted F1 score and kappa were similar for these three classifiers on the MS image. Something worth noting is that the kappa value for the DII_23 images was extremely low. This is a metric that take agreement beyond chance into account. However, Foody (2020) states that chance agreement is irrelevant in an accuracy assessment for remote sensing applications. Although it is embedded as a standard practise, many researchers now question the kappa coefficient because of various flaws in its argumentation (Pontius & Millones, 2011; Foody, 2020).

Several other researches concluded that the Support Vector Machine was the best performing classifier in comparison with other classifiers (Mederos-Barrera et al., 2022; Bangira et al., 2019; Wahidin et al., 2015; Cervantes et al., 2020). In this research, SVM also performs well in terms of accuracy, but also in terms of visual aspects. Each of the classes seem well represented in the classified image and the outcome is smooth in contrary to KNN and RT. In these two classifications of the water column corrected image DII_23, the so called salt-and-pepper effect can be observed. This is an occurrence of isolated pixels with high local spatial heterogeneity between neighbouring pixels (Hirayama, 2018). Even after performing smooth filtering, the noise was not reduced. The noise could be reduced with an object based classification using a segmented raster. However, this is a complicated procedure and summarizes the information, making no good use of the high-spatial resolution of this imagery (Hirayama, 2018).

5.4 Comparison between 2009 and 2018

Change detection is done by visually comparing structures between the years 2009 and 2018. Initially an attempt was done to perform a change detection with the use of classified rasters. However, there were discrepancies in the quality of the classified rasters. The success level of change detection of classified rasters depends on the reliability of the classified maps, meaning that errors in the individual classified maps are compounded (Vahtmäe et al., 2011). Therefore, it is decided to continue with visual inspection of change.

In Figure 26, a comparison is made between visible structures in the water of years 2009 and 2018. As can be seen in Fig 26A, C & D, some structures seem to not have changed much in 9 years. These could be rock formations covered in a type of substrate such as coral. Without knowledge of what these structures actually are and without classification with the use of spectral signatures, it is difficult to make statements on benthic cover change over time. If it shows geomorphological features of the seafloor, it could be used for predictive habitat mapping, since ecological models already exist for many geomorphically defined habitats (Harris, 2012).

In Fig 26B and in the lower part of 26C, dark patched fields have appeared. Again it can not be said with certainty what these patches are, but these could be algal fields. Increase in the amount of algae together with a decrease in coral is an indicator of declined reef quality (Souter et al., 2020) Therefore, it is important to monitor these areas closely. This also highlights the importance of up-to-date in-situ data, since these patches appeared in only 9 years.

6. Conclusions and recommendations

In this research, an attempt was made to map the benthic habitats around St. Eustatius. WorldView-3 imagery and training data were used to achieve this. In this section, an answer will be given to the three sub questions, finally answering the main question.

6.1 Sub questions

- 1- Which classification algorithms are most suitable for benthic habitat mapping of shallow waters (<30m)?

The classification algorithms that were compared in this research are the ISODATA unsupervised classification, Random Tree, K-Nearest Neighbor, Support Vector Machine and the Maximum Likelihood Classifier. ISODATA is an unsupervised algorithm and therefore does not use any training data. Although accuracies were lowest for this classifier, it could be useful prior to a field campaign to have an idea of the structures on the sea surface. All of the supervised classifiers had relatively good accuracies. MLC had the lowest accuracy of the four supervised classifications and the majority of the water column corrected image was classified as sand. K-NN and RT had a 'salt-and-pepper' effect in the water column corrected classification and a majority of the area here was classified as 'Coral & Gorgonian'. The only classifier that had a good representation of all three classes and did have a similar outcome for the multispectral image and the water column correction image was the Support Vector Machine. The classified image also did not change much after removing observations from the training data, showing it is not sensitive to an unequal division of observations over the classes.

- 2- What is the effect of correcting for water depth to benthic habitat classification of WV-3 imagery?

Water depth has a large effect on attenuation of light. Therefore, a water column correction was performed to minimize this influence. Because of striping in the red band, only the Depth-Invariant Indices of coastal with green & blue with green were compared to the original image. Identification of objects is expected to be better with a combination of more bands, since every pixel location then has more than one value associated with it. The blue and green Depth-Invariant Index showed clear visual improvement, but this was not translated into a higher accuracy. While water column correction using the coastal band resulted in a higher accuracy than with the blue band, it was still lower than the original image. However, the water column corrected image could be helpful with unsupervised classification, as it showed much more variation of patterns in the deeper part of the water.

- 3- Can change in the composition of benthic habitats be detected from WV imagery between 2009 and 2018?

To perform a change detection it is important to have high-resolution satellite imagery acquired during good weather conditions. Preprocessing steps can eliminate some effects of waves and sunglint, but change detection on classified rasters can only be performed if quality of both rasters is similar. However, visual change detection can be done if there is knowledge on the area and occurring benthic habitats on rock formations. Incorporating spectral signatures into the research by comparing classified rasters would be more valuable to detect changes in the composition of benthic habitats.

The main question for this research was “*To what extent can benthic habitats of St. Eustatius be accurately mapped using in situ data and WorldView-3 imagery?*”

It can be concluded that the quality of the data is most important for an accurate classification. Since weather conditions were calm at the moment the image from 2018 was captured, there were almost no waves and therefore not much sunglint visible. Also, since the image was already radiometrically corrected, no influence of the atmosphere was apparent and no clouds or shadows were obstructing area's of the water.

The overall accuracy for the classifications ranged from 33.3 to 67.3. As mentioned in chapter three, a classification accuracy above 60% is generally accepted for benthic habitat mapping of shallow waters. The accuracies of three classifiers were above 60%, so therefore can be accepted. Although the accuracies of the water column corrected images were under this threshold, structures in the water were very visible. Therefore, with good expert knowledge and interpretation, these maps can be useful for management and monitoring of the benthic habitats around St. Eustatius. In conclusion, integrating up-to-date in situ data with high-resolution satellite imagery has great potential to identify and classify the benthic habitats of St. Eustatius.

6.2 Recommendations

During this research there were some limitations that could use further research. Therefore, in this section the limitations are discussed and some suggestions are provided.

Field data

- The field survey dated from 2012/2013 while the satellite image from this research was from the year 2018. Optimally, the field data and satellite imagery would be from the same year to make sure the habitat type that is noted is still accurate. Therefore, it would be beneficial to have newer in-situ data.
- Some observation points in the eastern part of the water were not provided till a later stage in this thesis and were therefore not used for training and validation. It is recommended to include these in the future to have information on all sides of the island.
- In this research, the classification scheme was based on a spectral signatures and number of observations per class. Some classes did not have enough training points and were therefore excluded or merged to other classes. A more even distribution in training points could be beneficial for image classification

Methodology:

- In this research, water column correction was performed using Lyzenga (1981). This created a Depth-Invariant Index for each pair of spectral bands. Since bathymetric information is available, further research could gather information on optical properties of the water so the performance of another water column correction method could be tested such as Sagawa (2010).
- In this research, the yellow band (585-625) was not used for any classification. However, further into the research literature suggested that the yellow band has the best spectral separability between corals and seagrass. Therefore, I suggest including yellow in further research.
- Comparison of accuracy assessments was done with two metrics: Kappa and the weighted F1-score. Literature is very contradictive on the best method to compare confusion matrices. Therefore, a more elaborate study on metrics is beneficial to all benthic habitat studies.

General recommendation:

- There is a gap between information on benthic habitats in the field and spectral response recorded by the sensor (Wicaksono & Aryaguna, 2020). Closing this gap could improve classification of benthic habitats in the future.

7. References

- Abasolo, J., Eugenio, F., Marcello, J., Medina, A., Bermejo, J. A., & Arbelo, M. (2012). Atmospheric correction models for high resolution WorldView-2 multispectral imagery: A case study in Canary Islands, Spain.. *Proc SPIE*. 10.1117/12.974564.
- Arora, M., Gujrati, A., Chaudhury, N. R., & Patel, R. C. (2018). Benthic coverage and bottom topography of coral reef environment over Pirotan reef, Gulf of Kachchh region, India. *Geocarto International*, 34(10), 1089–1097. <https://doi.org/10.1080/10106049.2018.1469678>
- Bangira, T., Alfieri, S. M., Menenti, M., & Van Niekerk, A. (2019). Comparing thresholding with machine learning classifiers for mapping complex water. *Remote Sensing*, 11(11), 1351.
- Bervoets, T., 2010. Report on the Economic Valuation of St. Eustatius' Coral Reef Resources. Stenapa, Report. 40 pp
- Breiman, L. (2001). Random forests. *Machine learning*, 45, 5-32.
- Calvert, J., Strong, J. A., Service, M., McGonigle, C., & Quinn, R. (2015). An evaluation of supervised and unsupervised classification techniques for marine benthic habitat mapping using multibeam echosounder data. *ICES Journal of Marine Science*, 72(5), 1498-1513.
- Cervantes, J., Garcia-Lamont, F., Rodríguez-Mazahua, L., & Lopez, A. (2020). A comprehensive survey on support vector machine classification: Applications, challenges and trends. *Neurocomputing*, 408, 189-215.
- Chicco, D., & Jurman, G. (2020). The advantages of the Matthews correlation coefficient (MCC) over F1 score and accuracy in binary classification evaluation. *BMC genomics*, 21(1), 1-13.
- Contreras-Silva, A. I., López-Caloca, A. A., Tapia-Silva, F. O., & Cerdeira-Estrada, S. (2012). Satellite remote sensing of coral reef habitats mapping in shallow waters at banco chinchorro reefs, México: a classification approach. *Remote Sensing—Applications: InTech*: 331-354.
- Davies, M. R., & Piontek, S. (2017). The marine fishes of St. Eustatius, Dutch Caribbean. *Marine Biodiversity*, 47(1), 27–35. <https://doi.org/10.1007/s12526-016-0575-1>
- Debrot, A. O., Houtepen, E., Meesters, E. H., van Beek, I., Timmer, T., Boman, E., de Graaf, M., Dijkman, E., Hunting, E. R., & Ballantine, D. L. (2014). Habitat diversity and bio-diversity of the benthic seascapes of St. Eustatius. IMARES Report C078/14. www.imares.wur.nl
- Degenhardt, F., Seifert, S., & Szymczak, S. (2019). Evaluation of variable selection methods for random forests and omics data sets. *Briefings in Bioinformatics*, 20(2), 492–503. <https://doi.org/10.1093/bib/bbx124>
- Dhodhi, M. K., Saghri, J. A., Ahmad, I., & Ul-Mustafa, R. (1999). D-ISODATA: A Distributed Algorithm for Unsupervised Classification of Remotely Sensed Data on Network of Workstations. *Journal of Parallel and Distributed Computing*, 59(2), 280–301. <https://doi.org/10.1006/jpdc.1999.1573>
- DigitalGlobe. (2016). DigitalGlobe Atmospheric Compensation. Retrieved from http://digitalglobemarketing.s3.amazonaws.com/files/documents/AComp_WP_ACOMP.pdf
- Ding, H., Shi, J., Wang, Y., & Wei, L. (2015). An improved dark-object subtraction technique for atmospheric correction of Landsat 8. *SPIE: Remote Sensing Image Processing, Geographic Information Systems, and Other Applications*. 9815,128-135.
- Doxania, G. M. P., Lafazania, P., Pikridasb, C. & Tsakiri-Stratia, M. 2012. Shallow water bathymetry over variable bottom types using multispectral WorldView-2 Image International Archives of the Photogrammetry, Remote Sensing and Spatial Information Sciences, Vol XXXIX-B8
- Foo, S. A., & Asner, G. P. (2019). Scaling up coral reef restoration using remote sensing technology. *Frontiers in Marine Science*, 6(MAR). <https://doi.org/10.3389/fmars.2019.00079>

- Foody, G. M. (2023). Challenges in the real world use of classification accuracy metrics: From recall and precision to the Matthews correlation coefficient. *Plos one*, 18(10), e0291908.
- Ge, Q.Z., Chun Ling, Z., Qiong, L., Xian Hui, X., & Zhang, G. (2008). High efficient classification on remote sensing images based on SVM. *The International Archives of the Photogrammetry, Remote Sensing and Spatial Information Sciences*. Vol. XXXVII. Part B2.
- Glasl, B., Webster, N. S., & Bourne, D. G. (2017). Microbial indicators as a diagnostic tool for assessing water quality and climate stress in coral reef ecosystems. *Marine Biology* 164, 91. <https://doi.org/10.1007/s00227-017-3097-x>
- Graham, N. A. J., & Nash, K. L. (2013). The importance of structural complexity in coral reef ecosystems. *Coral Reefs*, 32(2), 315–326. <https://doi.org/10.1007/s00338-012-0984-y>
- Grandini, M., Bagli, E., & Visani, G. (2020). Metrics for multi-class classification: an overview. arXiv preprint arXiv:2008.05756.
- Green, E. P., Mumby, P. J., Edwards, A. J. & Clark, C. D. 2000. *Remote Sensing Handbook for Tropical Coastal Management*. Coastal Management Sourcebooks 3. Paris: UNESCO.
- Harris, P. T. (2012). From seafloor geomorphology to predictive habitat mapping: progress in applications of biophysical data to ocean management. https://proceedings.utwente.nl/239/1/Harris_extended_abstract.pdf.
- Hasan, R. C., Ierodiaconou, D., & Monk, J. (2012). Evaluation of four supervised learning methods for benthic habitat mapping using backscatter from multi-beam sonar. *Remote Sensing*, 4(11), 3427–3443. <https://doi.org/10.3390/rs4113427>
- Hedley, J. D., Harborne, A. R., & Mumby, P. J. (2005). Simple and robust removal of sun glint for mapping shallow-water benthos. *International Journal of Remote Sensing*, 26(10), 2107–2112. <https://doi.org/10.1080/01431160500034086>
- Hedley, J. D., Roelfsema, C., Brando, V., Giardino, C., Kutser, T., Phinn, S., Mumby, P. J., Barrilero, O., Laporte, J., & Koetz, B. (2018). Coral reef applications of Sentinel-2: Coverage, characteristics, bathymetry and benthic mapping with comparison to Landsat 8 The Sentinel-2A and 2B Multi-Spectral Instrument. *Remote Sensing of Environment*, 216, 598–614. <https://doi.org/10.1016/j.rse.2018.07.014>
- Hedley, J. D., Roelfsema, C. M., Phinn, S. R., & Mumby, P. J. (2012). Environmental and sensor limitations in optical remote sensing of coral reefs: Implications for monitoring and sensor design. *Remote Sensing*, 4(1), 271–302. <https://doi.org/10.3390/rs4010271>
- Hirayama, H., Sharma, R. C., Tomita, M., & Hara, K. (2019). Evaluating multiple classifier system for the reduction of salt-and-pepper noise in the classification of very-high-resolution satellite images. *International journal of remote sensing*, 40(7), 2542-2557.
- Hochberg, E. J., Atkinson, M. J., Apprill, A., & Andréfouët, S. (2003a). Spectral reflectance of coral. *Coral Reefs*, 23, 84–95. <https://doi.org/10.1007/s00338-003-0350-1>
- Hochberg, E. J., Atkinson, M. J., & Andréfouët, S. (2003b). Spectral reflectance of coral reef bottom-types worldwide and implications for coral reef remote sensing. *Remote Sensing of Environment*, 85, 159–173. [https://doi.org/10.1016/S0034-4257\(02\)00201-8](https://doi.org/10.1016/S0034-4257(02)00201-8)
- Janowski, L., Trzcinska, K., Tegowski, J., Kruss, A., Rucinska-Zjadacz, M., & Pocwiardowski, P. (2018). Nearshore benthic habitat mapping based on multi-frequency, multibeam echosounder data using a combined object-based approach: A case study from the Rowy Site in the Southern Baltic Sea. *Remote Sensing*, 10(12). <https://doi.org/10.3390/rs10121983>
- Kachelriess, D., Wegmann, M., Gollock, M., & Pettorelli, N. (2014). The application of remote sensing for marine protected area management. In *Ecological Indicators* (Vol. 36, pp. 169–177). <https://doi.org/10.1016/j.ecolind.2013.07.003>

- Kay, S., Hedley, J. D., & Lavender, S. (2009). Sun Glint Correction of High and Low Spatial Resolution Images of Aquatic Scenes: a Review of Methods for Visible and Near-Infrared Wavelengths. *Remote Sens*, 1, 697–730. <https://doi.org/10.3390/rs1040697>
- Keles, T., & Altun, M. (2016). Comparison of classical linear regression and orthogonal regression according to the sum of squares perpendicular distances. *Journal of Measurement and Evaluation in Education and Psychology*, 7(2), 296-308.
- Kuester, M. 2016. Radiometric Use of WorldView-3 Imagery. Technical note. Colorado, USA: Digital Globe.
- Kutser, T., Hedley, J., Giardino, C., Roelfsema, C., & Brando, V. E. (2020). Remote sensing of shallow waters – A 50 year retrospective and future directions. *Remote Sensing of Environment*, 240. <https://doi.org/10.1016/j.rse.2019.111619>
- Lam, V. W. Y., Chavanich, S., Djoundourian, S., Dupont, S., Gaill, F., Holzer, G., Isensee, K., Katua, S., Mars, F., Metian, M., & Hall-Spencer, J. M. (2019). Dealing with the effects of ocean acidification on coral reefs in the Indian Ocean and Asia. In *Regional Studies in Marine Science* (Vol. 28). Elsevier B.V. <https://doi.org/10.1016/j.rsma.2019.100560>
- Lebedev, N.E., Zapevalov, A.S. (2019). Modeling of a Sun Glint on a Sea Surface for Remote Sensing Purposes. *Physical and Mathematical Modeling of Earth and Environment Processes* (2018). Springer Proceedings in Earth and Environmental Sciences. Springer, Cham. https://doi.org/10.1007/978-3-030-11533-3_15
- Liu, D., & Xia, F. (2010). Assessing object-based classification: Advantages and limitations. *Remote Sensing Letters*, 1(4), 187–194. <https://doi.org/10.1080/01431161003743173>
- Lyzenga, D. R. (1981). Remote sensing of bottom reflectance and water attenuation parameters in shallow water using aircraft and Landsat data. *INT. J. Remote Sensing*, 2(1), 71–82.
- Mandlburger, G., Kremer, J., Steinbacher, F., & Baran, R. (2018). Investigating the use of coastal blue imagery for bathymetric mapping of inland water bodies. *The International Archives of the Photogrammetry, Remote Sensing and Spatial Information Sciences*, 42, 275-282.
- Manessa, M. D. M., Kanno, A., Sekine, M., Ampou, E. E., Widagti, N., & As-Syakur, A. R. (2014). Shallow-water benthic identification using multispectral satellite imagery: Investigation on the effects of improving noise correction method and spectral cover. *Remote Sensing*, 6(5), 4454–4472. <https://doi.org/10.3390/rs6054454>
- McIntyre, K., McLaren, K., & Prospere, K. (2017). Mapping shallow nearshore benthic features in a Caribbean marine-protected area: assessing the efficacy of using different data types (hydroacoustic versus satellite images) and classification techniques. *International Journal of Remote Sensing*, 39(4), 1117–1150. <https://doi.org/10.1080/01431161.2017.1395924>
- Mederos-Barrera, A., Marcello, J., Eugenio, F., & Hernández, E. (2022). Seagrass mapping using high resolution multispectral satellite imagery: A comparison of water column correction models. *International Journal of Applied Earth Observation and Geoinformation*, 113. <https://doi.org/10.1016/j.jag.2022.102990>
- Micallef, A., le Bas, T. P., Huvenne, V. A. I., Blondel, P., Hühnerbach, V., & Deidun, A. (2012). A multi-method approach for benthic habitat mapping of shallow coastal areas with high-resolution multibeam data. *Continental Shelf Research*, 39–40, 14–26. <https://doi.org/10.1016/j.csr.2012.03.008>
- Minghelli-Roman, A., Dupouy, C. (2014). Correction of the water column attenuation: Application to the seabed mapping of the lagoon of New Caledonia using MERIS images. *IEEE Journal of Selected Topics in Applied Earth Observations and Remote Sensing*, 7 (6), pp.2619-2629. [ff10.1109/JSTARS.2014.2307956ff](https://doi.org/10.1109/JSTARS.2014.2307956).
- Mishra, D., Narumalani, S., Rundquist, D., & Lawson, M. (2006). Benthic Habitat Mapping in Tropical Marine Environments Using QuickBird Multispectral Data. *PE&RS* 72(9), 1037-1048.
- Moberg, F., & Folke, C. (1999). Ecological goods and services of coral reef ecosystems. In *Ecological Economics*. *Ecological economics*, 29(2), 215-233.

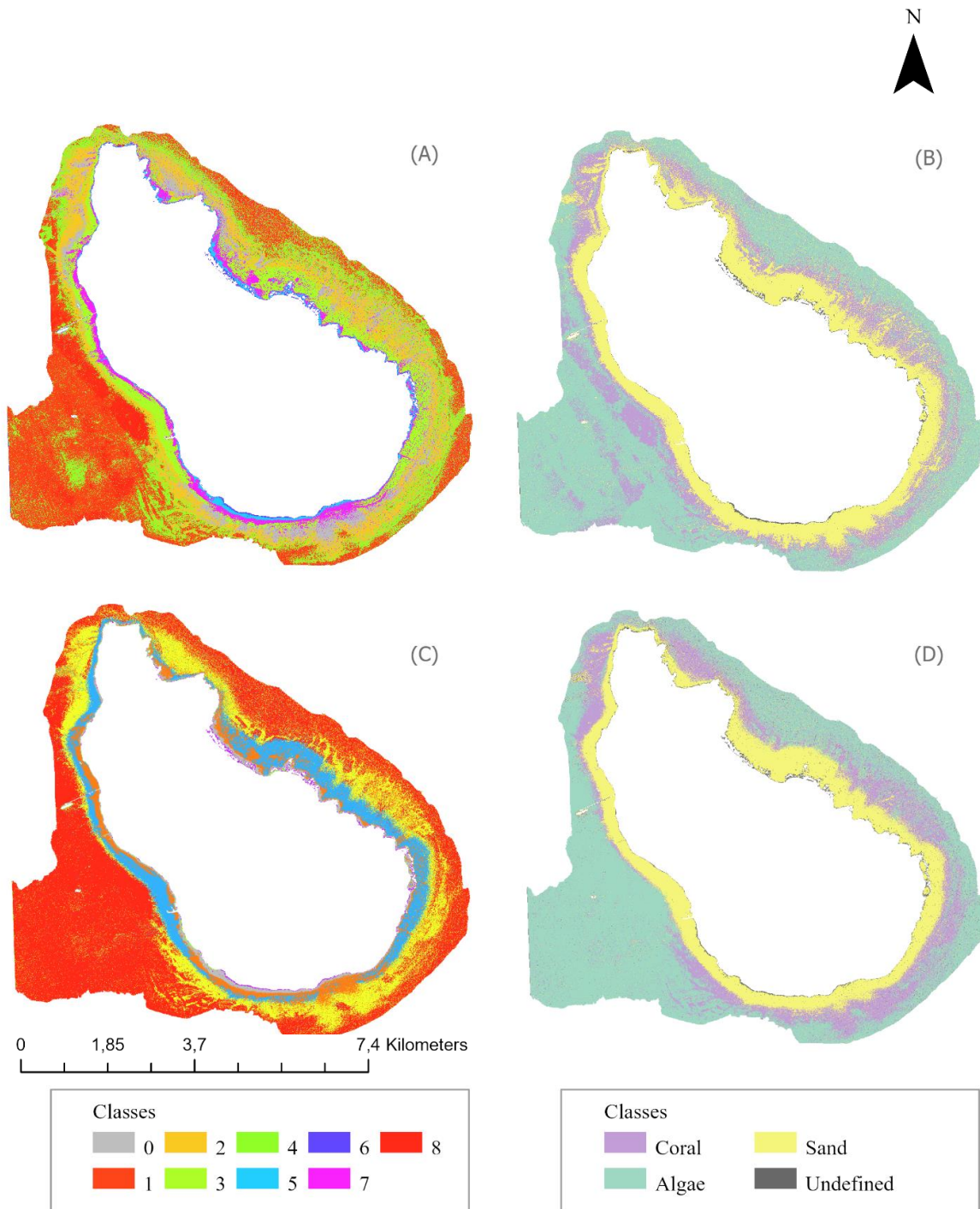
- Mohamed, H., Nadaoka, K., & Nakamura, T. (2018). Assessment of machine learning algorithms for automatic benthic cover monitoring and mapping using towed underwater video camera and high-resolution satellite images. *Remote Sensing*, 10(5). <https://doi.org/10.3390/rs10050773>
- Mumby, P. J., Clark, C. D., Green, E. P., & Edwards, A. J. (1997). Benefits of water column correction and contextual editing for mapping coral reefs. *Int. j. Remote Sensing*, 19(1), 203–210.
- Mumby, P. J., Skirving, W., Strong, A. E., Hardy, J. T., LeDrew, E. F., Hochberg, E. J., Stumpf, R. P., & David, L. T. (2004). Remote sensing of coral reefs and their physical environment. *Marine Pollution Bulletin*, 48(3–4), 219–228. <https://doi.org/10.1016/j.marpolbul.2003.10.031>
- O’Neill, J. D., Costa, M., & Sharma, T. (2011). Remote sensing of shallow coastal benthic substrates: In situ spectra and mapping of eelgrass (*Zostera marina*) in the Gulf Islands National Park Reserve of Canada. *Remote Sensing*, 3(5), 975–1005. <https://doi.org/10.3390/rs3050975>
- Opitz, J. (2022). From Bias and Prevalence to Macro F1, Kappa, and MCC: A structured overview of metrics for multi-class evaluation. Heidelberg University. https://www.cl.uni-heidelberg.de/~opitz/pdf/metric_overview.pdf
- Otukei, J. R., & Blaschke, T. (2010). Land cover change assessment using decision trees, support vector machines and maximum likelihood classification algorithms. *International Journal of Applied Earth Observation and Geoinformation*, 12(SUPPL. 1). <https://doi.org/10.1016/j.jag.2009.11.002>
- Perumal, K., & Bhaskaran, R. (2010). Supervised classification performance of multispectral images. arXiv preprint arXiv:1002.4046.
- Pommé, L. E., Bourqui, R., Giot, R., & Auber, D. (2022). Relative Confusion Matrix: Efficient Comparison of Decision Models. In 2022 26th International Conference Information Visualisation (IV) (pp. 98-103). IEEE.
- Pontius Jr, R. G., & Millones, M. (2011). Death to Kappa: birth of quantity disagreement and allocation disagreement for accuracy assessment. *International Journal of Remote Sensing*, 32(15), 4407-4429.
- Prajwala, T. R. (2015). A Comparative Study on Decision Tree and Random Forest Using R Tool. *IJARCCCE*, 4(1), 196–199. <https://doi.org/10.17148/ijarccce.2015.4142>
- Rowan, G. S. L., & Kalacska, M. (2021). A review of remote sensing of submerged aquatic vegetation for non-specialists. In *Remote Sensing* (Vol. 13, Issue 4, pp. 1–50). MDPI AG. <https://doi.org/10.3390/rs13040623>
- Sagawa, T.; Boisnier, E.; Komatsu, T.; Mustapha, K.B.; Hattour, A.; Kosaka, N.; Miyazaki, A. Using bottom surface reflectance to map coastal marine areas: A new application method for Lyzenga’s model. *Int. J. Remote Sens.* 2010, 31, 3051–3064.
- Setlawan, K.T., Winarso, G., Ibrahim, A., Purwanto, A.D. & Parsa, I.M. (2022). Comparative analysis of classification methods for mapping shallow water habitats using SPOT-7 Satellite imagery in Nusa Lembongan Island, Bali. *International Journal of Remote Sensing and Earth Sciences* 19 (01).
- Smith, J. (2008). In-water monitoring of sea turtle aggregations in St. Eustatius National Marine Park. http://www.widecast.org/What/Country/Eustatius/Docs/In_Water_Monitoring_of_Sea_Turtle_Aggregations_in_St_Eu_statius.pdf
- Souter, D., Planes, S., Wicquart, J., Logan, M., Obura, D. & Staub, F. (2020) Status of coral reefs of the world: 2020. In *Global Coral Reef Monitoring Network; Int. Coral Reef Initiative*. Australian Institute of Marine Science.
- Tyagi, P. & Bhosle, U. (2011). Atmospheric Correction of Remotely Sensed Images in Spatial and Transform Domain. *International Journal of Image Processing*. 5(5), 564-578
- Vahtmäe, E., Kutser, T., Kotta, J., & Pärnoja, M. (2011). Detecting patterns and changes in a complex benthic environment of the Baltic Sea. *Journal of Applied Remote Sensing*, 5(1), 053559-053559.
- Wahidin, N., Siregar, V. P., Nababan, B., Jaya, I., & Wouthuyzen, S. (2015). Object-based Image Analysis for Coral Reef Benthic Habitat Mapping with Several Classification Algorithms. *Procedia Environmental Sciences*, 24, 222–227. <https://doi.org/10.1016/j.proenv.2015.03.029>

- Wicaksono, P., & Aryaguna, P. A. (2020). Analyses of inter-class spectral separability and classification accuracy of benthic habitat mapping using multispectral image. *Remote Sensing Applications: Society and Environment*, 19, 100335.
- Wicaksono, P., Aryaguna, P. A., & Lazuardi, W. (2019). Benthic habitat mapping model and cross validation using machine-learning classification algorithms. *Remote Sensing*, 11(11). <https://doi.org/10.3390/rs11111279>
- Wilkinson, C., Souter, D. (2008). Status of Caribbean coral reefs after bleaching and hurricanes in 2005. Global Coral Reef Monitoring Network, and Reef and Rainforest Research Centre, Townsville, 152 p.
- Xu, H., Liu, Z., Zhu, J., Lu, X., & Liu, Q. (2019). Classification of Coral Reef Benthos around Ganquan Island Using WorldView-2 Satellite Imagery. *Journal of Coastal Research*, 93(sp1), 466–474. <https://doi.org/10.2112/SI93-061.1>
- Zhang, C., Selch, D., Xie, Z., Roberts, C., Cooper, H., & Chen, G. (2013). Object-based benthic habitat mapping in the Florida Keys from hyperspectral imagery. *Estuarine, Coastal and Shelf Science* 134, 88-97. <https://doi.org/10.1016/j.ecss.2013.09.018>
- Zoffoli, M. L., Frouin, R., & Kampel, M. (2014). Water column correction for coral reef studies by remote sensing. In *Sensors* 14, 16881–16931. MDPI AG. <https://doi.org/10.3390/s140916881>

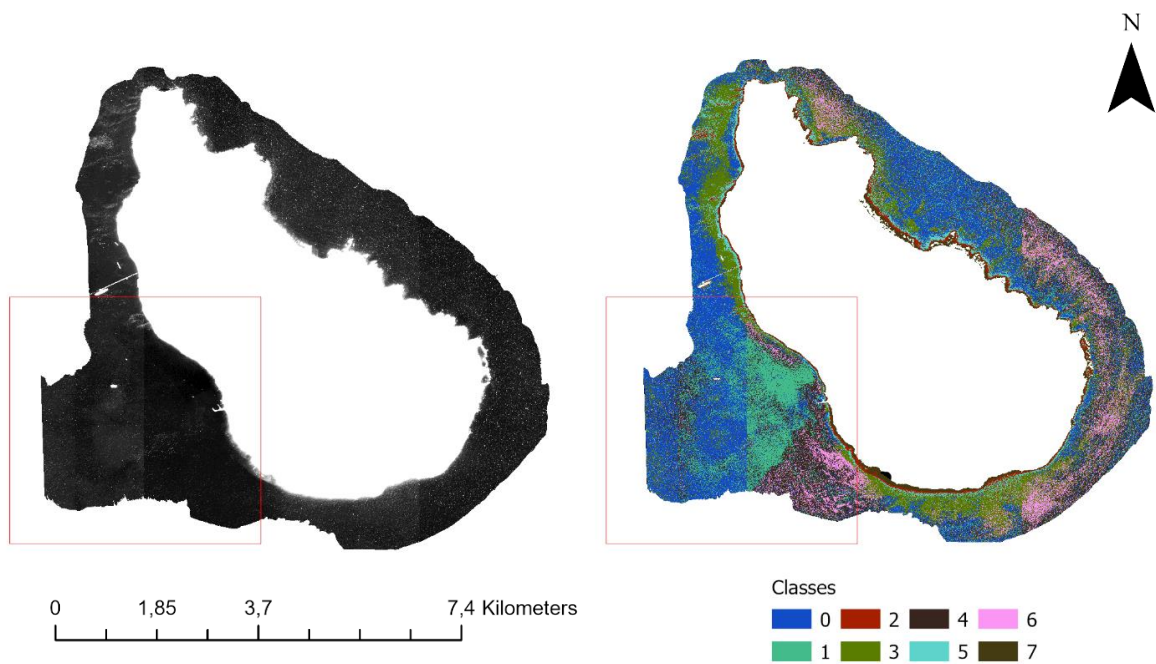
8. Appendices

Appendix A - Results of the ISODATA classification.

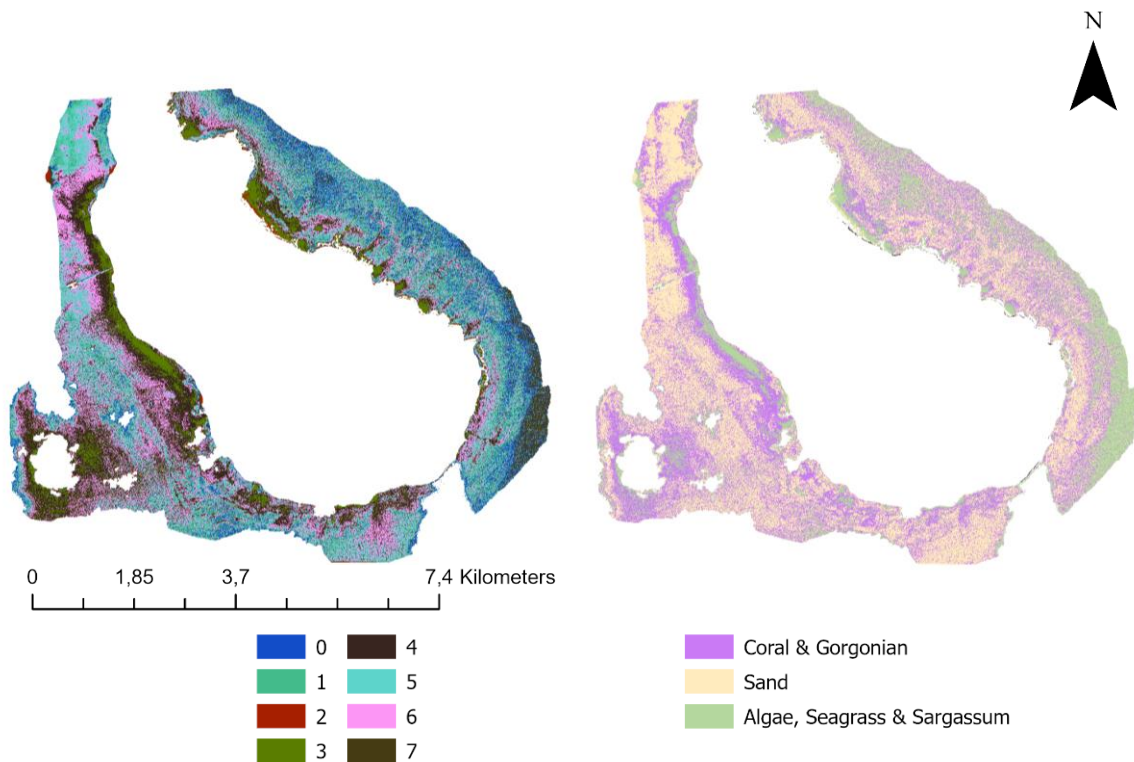
A&B are before sunlint removal, C&D are after sunlint removal. The left side is before assigning classes, the right side is after assigning classes.



Appendix B – RGB image and ISODATA classification after water column correction



Appendix C – ISODATA classification of 2009 imagery after sunglint removal



Appendix D - Confusion matrices for five classifiers

ISODATA

MS

	C1	C2	C3	Total
C1	26	21	3	50
C2	20	10	2	32
C3	33	12	26	71
Total	79	43	31	153

C1 is Coral & Gorgonian, C2 is sand C3 is Algae, Seagrass & Sargassum

DII_23_5x5

	C1	C2	C3	Total
C1	40	26	15	81
C2	11	8	4	23
C3	28	9	12	49
Total	79	43	31	153

C1 is Coral & Gorgonian, C2 is sand C3 is Algae, Seagrass & Sargassum

MLC

MS_3x3

	C1	C2	C3	Total
C1	43	10	10	63
C2	15	26	3	44
C3	21	7	18	46
Total	79	43	31	153

C1 is Coral & Gorgonian, C2 is sand C3 is Algae, Seagrass & Sargassum

DII_23

	C1	C2	C3	Total
C1	14	9	3	26
C2	23	19	10	52
C3	42	15	18	75
Total	79	43	31	153

C1 is Coral & Gorgonian, C2 is sand C3 is Algae, Seagrass & Sargassum

K-NN

MS_5x5

	C1	C2	C3	Total
C1	64	12	16	92
C2	10	24	3	37
C3	5	7	12	24
Total	79	43	31	153

C1 is Coral & Gorgonian, C2 is sand C3 is Algae, Seagrass & Sargassum

DII_23

	C1	C2	C3	Total
C1	44	24	13	81
C2	18	10	4	32
C3	17	9	14	40
Total	79	43	31	153

C1 is Coral & Gorgonian, C2 is sand C3 is Algae, Seagrass & Sargassum

SVM

MS_5x5

	C1	C2	C3	Total
C1	44	7	5	56
C2	12	30	4	46
C3	23	6	22	51
Total	79	43	31	153

C1 is Coral & Gorgonian, C2 is sand C3 is Algae, Seagrass & Sargassum

DII_23_5x5

	C1	C2	C3	Total
C1	26	10	10	46
C2	24	25	9	58
C3	29	8	12	49
Total	79	43	31	153

*C1 is Coral & Gorgonian, C2 is sand C3 is Algae, Seagrass & Sargassum***RT**

MS_5x5

	C1	C2	C3	Total
C1	61	15	8	84
C2	8	22	3	33
C3	10	6	20	36
Total	79	43	31	153

C1 is Coral & Gorgonian, C2 is sand C3 is Algae, Seagrass & Sargassum

DII_23_5x5

	C1	C2	C3	Total
C1	28	18	15	61
C2	24	20	5	49
C3	27	5	11	43
Total	79	43	31	153

C1 is Coral & Gorgonian, C2 is sand C3 is Algae, Seagrass & Sargassum